Phased and phaseless domain reconstruction in inverse scattering problem via scattering coefficients

H. Ammari and Y.T. Chow and J. Zou

Phased and phaseless domain reconstruction in inverse scattering problem via scattering coefficients

Habib Ammari[*]   Yat Tin Chow[†]   Jun Zou[‡]

Abstract

In this work we shall review the (phased) inverse scattering problem and then pursue the phaseless reconstruction from far-field data with the help of the concept of scattering coefficients. We perform sensitivity, resolution and stability analysis of both phased and phaseless problems and compare the degree of ill-posedness of the phased and phaseless reconstructions. The phaseless reconstruction is highly nonlinear and much more severely ill-posed. Algorithms are provided to solve both the phased and phaseless reconstructions in the linearized case. Stability is studied by estimating the condition number of the inversion process for both the phased and phaseless cases. An optimal strategy is suggested to attain the infimum of the condition numbers of the phaseless reconstruction, which may provide an important guidance for efficient phaseless measurements in practical applications. To the best of our knowledge, the stability analysis in terms of condition numbers are new for the phased and phaseless inverse scattering problems, and are very important to help us understand the degree of ill-posedness of these inverse problems. Numerical experiments are provided to illustrate the theoretical asymptotic behavior, as well as the effectiveness and robustness of the phaseless reconstruction algorithm.

1 Introduction

The inverse scattering problems are well known to be severely ill-posed. It has widespread applications in, e.g., oil/crack detection, target identification, geophysical prospection, non-destructive testing, medical imaging, physiological measurement [3, 4, 19, 33, 34, 35, 41, 42, 44, 45, 46, 50, 51]. Due to their applications, inverse scattering problems have attracted much attention, and many numerical algorithms have been developed over the recent decades for phased reconstruction problems, e.g., time-reversal multiple signal classification methods [25, 39], the contrast source inversion methods [2, 3, 4, 44, 45, 46, 47], the continuation method [10], the subspace-based optimization method [15, 16], the linear sampling or probing methods [17, 31, 40], the parallel radial bisection method [36], direct sampling methods [23], multi-level sampling methods [31, 37], etc.

However, in many areas of applied sciences it is very difficult and expensive to obtain the phased data of the scattered field, while the phaseless data is much easier to acquire. In addition, the phase of the field is more easily polluted by the noise than the amplitude in many practical situations. For instance, the measurement of the phase is extremely difficult when the working frequency is beyond tens of gigahertz, and one can not expect a good accuracy of the phase measurement [34, 35, 41]. This motivates the phaseless reconstructions, and attracts huge attention from both the physics and mathematics communities. Nonetheless, the phaseless reconstruction is yet much more severely ill-posed than the phased

---

[*]Department of Mathematics, ETH Zürich, Rämistrasse 101, CH-8092 Zürich, Switzerland. The work of this author was supported by the ERC Advanced Grant Project MULTIMOD–267184. (habib.ammari@math.ethz.ch).

[†]Department of Mathematics, University of California, Los Angeles, CA 90095-1555, USA. (ytchow@math.cuhk.edu.hk).

[‡]Department of Mathematics, Chinese University of Hong Kong, Shatin, N.T., Hong Kong. The work of this author was substantially supported by Hong Kong RGC grants (projects 14306814 and 405513). (zou@math.cuhk.edu.hk).

reconstruction, in particular, it appears to be impossible to recover the location of an obstacle only from the modulus of the far-field pattern owing to the fact that it is invariant under translations [30]. In spite of this drastic difficulty, several approaches have been proposed in literature for the phaseless medium reconstruction in optics, acoustic and electromagnetics, e.g., the phaseless data multiplicative regularized contrast sources inversion method [33, 52], and several other methods [14, 18, 22, 34, 35, 41, 53]. Also, the phaseless acoustic (sound-soft) obstacle reconstruction was studied in [24], where the reconstruction is split into two parts: the shape reconstruction from the phaseless data and the location of the obstacle from a few phased measurements. Theoretically, the uniqueness of a phaseless scattering reconstruction was established in [26, 27], while the phaseless measurements were connected to the Radon transform of the potential under the Born approximation [29], and a new numerical method was proposed in [28] for the phaseless problem using this connection to Radon transform. There are also other works which address both the theoretical and algorithmic aspects of problems related to phaseless reconstruction of a function or vector, where the phase of a function or vector is recovered from the modulus of its evaluation of a special family of functionals [13, 21, 38], e.g., the coefficients of a Cauchy wavelet transform.

In this work, we shall study both the phased and phaseless shape reconstructions from the far-field data of an acoustic medium scattering problem, so the governing equation of our interest is the following Helmholtz system:

$$\Delta u + k^2(1 + q(x)) u = 0 \quad \text{in} \quad \mathbb{R}^2 \tag{1.1}$$

where u is the total field, $q(x) \geq 0$ is the contrast of the medium and k is the wave number.

Suppose that D is an inclusion contained inside a homogeneous background medium, and it is an open bounded connected domain with a $\mathcal{C}^{1,\alpha}$-boundary for $0 < \alpha < 1$. We consider the contrast q of the form

$$q(x) = \varepsilon^* \chi_D(x), \tag{1.2}$$

where χ_D is the characteristic function of D and $\varepsilon^* > 0$ is a constant. The Helmholtz system (1.1) is often complemented by the physical outgoing Sommerfeld radiation condition:

$$\left| \frac{\partial}{\partial |x|} u^s - iku^s \right| = O(|x|^{-\frac{3}{2}}) \quad \text{as} \quad |x| \to \infty \,, \tag{1.3}$$

where $u^s := u - u^i$ is the scattered field and u^i is the incident wave. Now we can see that the solution u to the system (1.1)-(1.3) represents the total field due to the scattering from the inclusion D corresponding to the incident u^i. Then the phased reconstruction is to recover the shape of D from the phased measurements of either the scattered field or the far-field, while the phaseless reconstruction is to recover the shape of D from only the magnitude of the scattered field or the far-field.

We shall analyse the sensitivity, resolution and stability of both phased and phaseless reconstructions in the linearized cases under certain measurement strategies, and compare the major differences between these two reconstructions. With the help of these analyses, we will propose an efficient measurement method which leads to a well-posed inversion process of the phaseless reconstruction. As demonstrated by our early works [6, 8, 9], the scattering coefficients provide a powerful and efficient tool for shape classification of a target domain, and this concept will also persist in this work to help us establish stable reconstruction algorithms and their analysis.

We start by recalling the phased reconstruction in the linearized case so as to provide important insight into the highly nonlinear phaseless reconstruction problems. Within this framework, we shall provide a resolution analysis on numerical reconstruction with phased data in terms of SNR, then propose algorithms for shape reconstructions with the phased measurement. Another major focus of this work is the stability of the phaseless reconstruction, for which we will provide an efficient algorithm, and estimate the condition number of the phaseless inversion process. We are able to establish a sharp upper bound for the infimum of the condition numbers of the inversion process over all phaseless measurement strategies for a given target resolution, hence propose an optimal modulus measurement method. A similar analysis is carried out for the phased reconstruction to allow a clear comparison between the phased and phaseless reconstructions. To the best of our knowledge, our stability estimates in terms of condition numbers are completely new to inverse medium scattering problems and appear to be a very important and effective novel tool to help us better understand the degree of ill-posedness and stability of both the phased and phaseless reconstructions.

The remaining part of the work is organized as follows. In section 2, we review the concept of scattering coefficients and obtain several important results, which will be of crucial importance to connect the scattering coefficients to both the phased and phaseless reconstructions, and help us develop efficient algorithms and their analysis. Then we move on to the sensitivity analysis of the phased measurement data in section 3, which will also give a link-up between the phaseless data and information about the shape of the domain. An important comparison is provided in section 3 for the similarities and differences between the phased and phaseless reconstructions. A phased reconstruction algorithm in the linearized case is then proposed in section 4, also with a clear resolution analysis of the algorithm. This resolution analysis is very helpful for us to understand the corresponding resolution constraint in the phaseless reconstruction. Next, we introduce our phaseless recovery problem in section 5, and provide a phaseless shape reconstruction algorithm in section 6. A stability analysis is performed for our new phaseless reconstruction algorithm in section 7, optimal strategies for minimizing the condition number of the inversion process and analysis of the differences between the ill-posed natures of the phased and phaseless reconstruction are also given. Numerical experiments are presented in section 8 to confirm the theoretical estimates of the condition number of our inversion process, and illustrate the effectiveness and robustness of our newly-proposed phaseless recovery algorithm. We emphasize that, although our analyses are performed only for two dimensions, similar results and analysis can be extended to higher dimensions as well.

2 Revisit to the concept of scattering coefficients and its sensitivity analysis

In this section, we recall the definition of the scattering coefficient [5, 6, 8] and provide some useful results about sensitivity analysis for our subsequent shape reconstruction. To do so, we first introduce some useful notation [6, 8]. Let Φ_k be the fundamental solution to the Helmholtz equation:

$$(\Delta + k^2)\,\Phi_k(x) = \delta_0(x), \tag{2.1}$$

where δ_0 is the Dirac mass at 0, with the outgoing Sommerfeld radiation condition:

$$\Big|\frac{\partial}{\partial |x|}\Phi_k - ik\Phi_k\Big| = O(|x|^{-\frac{3}{2}}) \quad \text{as} \quad |x| \to \infty\,.$$

Then Φ_k can be written in terms of the Hankel function $H_0^{(1)}$ of the first kind of order zero:

$$\Phi_k(x) = -\frac{i}{4}H_0^{(1)}(k|x|)\,. \tag{2.2}$$

Given an incident field u^i satisfying the homogeneous Helmholtz equation:

$$\Delta u^i + k^2 u^i = 0\,, \tag{2.3}$$

then the solution u to (1.1) and (1.3) can be represented by the Lippmann-Schwinger equation as

$$u(x) = u^i(x) - \varepsilon^* k^2 \int_D \Phi_k(x-y)u(y)dy\,, \quad x \in \mathbb{R}^2\,, \tag{2.4}$$

and the scattered field is given by

$$u^s(x) = -\varepsilon^* k^2 \int_D \Phi_k(x-y)u(y)dy\,, \quad x \in \mathbb{R}^2\,. \tag{2.5}$$

In what follows, we shall often use the following single-layer potential:

$$S_{\partial D}^k[\phi](x) = \int_{\partial D} \Phi_k(x-y)\phi(y)\,ds(y)\,, \quad \phi \in L^2(\partial D), \tag{2.6}$$

then the scattering coefficients are defined as follows [6, 8]:

3

Definition 2.1. *For $n, m \in \mathbb{Z}$, we define the scattering coefficient $W_{nm}(D, \varepsilon^*, k)$ as*

$$W_{nm}(D, \varepsilon^*, k) = \int_{\partial\Omega} J_n(kr_x) e^{-in\theta_x} \phi_m(x) \, ds(x), \tag{2.7}$$

where $x = r_x(\cos\theta_x, \sin\theta_x)$ is in polar coordinates and the weight function $\phi_m \in L^2(\partial D)$ is such that the pair $(\phi_m, \psi_m) \in L^2(\partial D) \times L^2(\partial D)$ satisfies the following system of integral equations:

$$\begin{cases} S_{\partial D}^{k\sqrt{\varepsilon^*+1}}[\phi_m](x) - S_{\partial D}^k[\psi_m](x) = J_m(kr_x)e^{im\theta_x}, \\ \frac{\partial}{\partial\nu} S_{\partial D}^{k\sqrt{\varepsilon^*+1}}[\phi_m](x) \mid_- - \frac{\partial}{\partial\nu} S_{\partial D}^k[\psi_m](x) \mid_+ = \frac{\partial}{\partial\nu}(J_m(kr_x)e^{im\theta_x}). \end{cases} \tag{2.8}$$

Here $+$ and $-$ in the subscripts indicate respectively the limits from outside D and inside D to ∂D along the normal direction, and $\partial/\partial\nu$ denotes the outward normal derivative.

The scattering coefficients $W_{nm}(D, \varepsilon^*, k)$ are basically the Fourier coefficients of the far-field pattern (a.k.a. the scattering amplitude), which is a 2π-periodic function in two dimensions [5, 6, 8]. For the incident field $e^{ik\hat{d}\cdot x}$ with a unit vector $\hat{d}$, we have

$$(u - u^i)(x) = ie^{-\pi i/4} \frac{e^{ik|x|}}{\sqrt{8\pi k|x|}} A_\infty(\hat{d}, \hat{x}, k) + O(|x|^{-\frac{3}{2}}) \quad \text{as } |x| \to \infty,$$

where $\hat{x} = x/|x| = (\cos\theta_x, \sin\theta_x)$ and $\hat{d} = (\cos\theta_d, \sin\theta_d)$ are in polar coordinates, and $A(\theta_d, \theta_x, k) := A_\infty(\hat{d}, \hat{x}, k)$ is the so-called far-field pattern. The following results can be found in [5, 6, 8].

Theorem 2.2. *Let $\mathfrak{F}_{\theta_d, \theta_x}[A(\theta_d, \theta_x, k)](m, n)$ be the (m, n)-th Fourier coefficient of the far-field pattern $A(\theta_d, \theta_x, k)$ with the background wave-number k, then it holds that*

$$W_{nm}(D, \varepsilon^*, k) = i^{(n-m)} \mathfrak{F}_{\theta_d, \theta_x}[A(\theta_d, \theta_x, k)](-m, n), \tag{2.9}$$

or equivalently,

$$A(\theta_d, \theta_x, k) = \sum_{m,n \in \mathbb{Z}} i^{(m-n)} e^{-im\theta_d} e^{in\theta_x} W_{nm}(D, \varepsilon^*, k). \tag{2.10}$$

The following result is a direct consequence of Corollary 7.1 in [6].

Theorem 2.3. *When the contrast ε^* is small, it holds that*

$$W_{nm}(D, \varepsilon^*, k) = \varepsilon^* k^2 \int_D J_n(kr) J_m(kr) e^{i(n-m)\theta} \, dx + O(\varepsilon^{*2}), \tag{2.11}$$

which can be simplified for the special case of domain D being the circular shape $D = B_R(0)$:

$$W_{nm}(B, \varepsilon^*, k) = 2\pi\varepsilon^* \delta_{nm} k^2 \int_0^R [J_n(kr)]^2 r dr + O(\varepsilon^{*2}). \tag{2.12}$$

We remark that the integral appearing in (2.12) can be calculated explicitly as a Lommel's integral, and this fact will become very helpful in section 3.

Before going to the discussion about the phased and phaseless reconstructions, we shall first provide an estimate of the scattering coefficient under a perturbation of an open ball $B_R(0)$, which is important for our subsequent analysis about the resolution of both the phased and phaseless reconstructions.

Let $\nu(x)$ be the outward unit normal to ∂B, and $D := B^\delta$ a δ-perturbation of $B := B_R(0)$ along the variational direction $h \in C^1(\partial D)$ with $||h|| = 1$:

$$\partial B^\delta := \{\tilde{x} = x + \delta h(x)\nu(x) : x \in \partial B\}, \tag{2.13}$$

then we can write the difference between the integrals over the domains B and B^δ for an L^1 function f:

$$\int_{B^\delta} f(x)dx - \int_B f(x)dx = \delta \int_{\partial B} f(x)h(x) \, ds(x) + O(\delta^2).$$

4

Now it follows from this and (2.11) that

$$W_{nm}(B^\delta, \varepsilon^*, k) - W_{nm}(B, \varepsilon^*, k)$$

$$= \varepsilon^* k^2 \int_{B^\delta \cup B \setminus B^\delta \cap B} \operatorname{sgn}(h) J_n(kr) J_m(kr) e^{i(n-m)\theta} \, dx + O\left(\varepsilon^* \delta^2 + \varepsilon^{*2}\right)$$

$$= \varepsilon^* \delta k^2 \int_{\partial B} h(x) J_n(kr) J_m(kr) e^{i(n-m)\theta} \, dx + O\left(\varepsilon^* \delta^2 + \varepsilon^{*2}\right)$$

$$= \varepsilon^* R \delta k^2 J_n(kR) J_m(kR) \int_0^{2\pi} h(\theta) e^{i(n-m)\theta} \, d\theta + O\left(\varepsilon^* \delta^2 + \varepsilon^{*2}\right)$$

$$= 2\pi R k^2 \varepsilon^* \delta J_n(kR) J_m(kR) \mathfrak{F}[h](n-m) + + O\left(\varepsilon^* \delta^2 + \varepsilon^{*2}\right),$$

where $\mathfrak{F}[h](n-m)$ stands for the $(n-m)$-th Fourier coefficient of the perturbation h in the argument θ.

If we further requires that the magnitude of δ is larger than ε^* in a way such that $\delta = (\varepsilon^*)^\alpha$ for some $0 < \alpha < 1$, then we arrive at the following result by some similar argument to the one in [5].

Theorem 2.4. *Let $D := B^\delta$ be a δ-perturbation of $B := B_R(0)$ as defined in (2.13), then it holds for $\delta = (\varepsilon^*)^\alpha$ with $0 < \alpha < 1$ that*

$$W_{nm}(B^\delta, \varepsilon^*, k) - W_{nm}(B, \varepsilon^*, k) = 2\pi R k^2 (\varepsilon^*)^{1+\alpha} J_n(kR) J_m(kR) \mathfrak{F}[h](n-m) + O(\varepsilon^*)^2. \qquad (2.14)$$

3 Sensitivity analysis of the phased measurement data

In this section, we shall develop a sensitivity analysis of the phased measurement of the far-field data based on the result for the scattering coefficients in Theorem 2.4. This shall help us provide a crucial expression between the phaseless measurement of the far-field data (i.e., only its magnitude) and the shape D.

Suppose that $D := B^\delta$ is a δ-perturbation of $B := B_R(0)$ along the variational direction $h \in C^1(\partial D)$ with $||h|| = 1$ as described earlier. Then it follows from (2.10), (2.12) and (2.14) that

$$A_\infty(\theta, \widetilde{\theta}, k)$$

$$= \sum_{n,m \in \mathbb{Z}} i^{n-m} e^{in\theta} e^{-im\widetilde{\theta}} W_{nm}(B^\delta, \varepsilon^*, k)$$

$$= 2\pi \varepsilon^* k^2 \sum_{l \in \mathbb{Z}} e^{il(\theta - \widetilde{\theta})} \int_0^R [J_l(kr)]^2 r \, dr + 2\pi R (\varepsilon^*)^{1+\alpha} k^2 \sum_{n,l \in \mathbb{Z}} i^l e^{il\widetilde{\theta}} e^{in(\theta - \widetilde{\theta})} J_n(kR) J_{n-l}(kR) \mathfrak{F}[h](l) + O(\varepsilon^*)^2.$$

Although the above expression looks quite complicated, it can be greatly simplified by some well-known properties of the Bessel functions. In fact, using the following form of the Graf's addition formula [48]:

$$\sum_{n=-\infty}^{\infty} J_n(x) J_{n-l}(y) e^{in\theta} = (-1)^l \left(\frac{x - y\exp(-i\theta)}{x - y\exp(i\theta)} \right)^{l/2} J_l\left(\sqrt{x^2 + y^2 - 2xy\cos(\theta)} \right) \qquad (3.1)$$

for $x, y > 0$ and $x \neq y$, and the well-known property for the second Lommel's integral:

$$\int_0^R [J_l(kr)]^2 r \, dr = \frac{R^2}{2} [J_l(kR)^2 - J_{l-1}(kR) J_{l+1}(kR)], \qquad (3.2)$$

we can significantly simplify the above expression of the far-field pattern as

$$A_\infty(\theta, \widetilde{\theta}, k) = \pi R^2 \varepsilon^* k^2 \sum_{l \in \mathbb{Z}} e^{il(\theta - \widetilde{\theta})} [J_l(kR)^2 - J_{l-1}(kR) J_{l+1}(kR)]$$

$$+ 2\pi R (\varepsilon^*)^{1+\alpha} k^2 \sum_{n,l \in \mathbb{Z}} i^l e^{il\widetilde{\theta}} e^{in(\theta - \widetilde{\theta})} J_n(kR) J_{n-l}(kR) \mathfrak{F}[h](l) + O(\varepsilon^*)^2$$

$$= \pi R^2 \varepsilon^* k^2 [J_0(2kR \sin((\widetilde{\theta} - \theta)/2)) - J_2(2kR \sin((\widetilde{\theta} - \theta)/2))]$$

$$+ 2\pi R (\varepsilon^*)^{1+\alpha} k^2 \sum_{l \in \mathbb{Z}} (-i)^l e^{il(\widetilde{\theta} + \theta)/2} J_l(2kR \sin((\widetilde{\theta} - \theta)/2)) \mathfrak{F}[h](l) + O(\varepsilon^*)^2. \qquad (3.3)$$

5

An interesting point to note is that the constants πR^2 and $2\pi R$ in front of the two terms ε^* and $(\varepsilon^*)^{1+\alpha}$ are respectively the volume and surface area of the open ball of radius R.

Summarizing the above discussions, we come directly to the following theorem.

Theorem 3.1. *If $\delta = (\varepsilon^*)^\alpha$ for $0 < \alpha < 1$, then*

$$A_\infty(\theta, \widetilde{\theta}, k) = \pi R^2 \varepsilon^* k^2 P_R(\theta, \widetilde{\theta}, k) + 2\pi R (\varepsilon^*)^{1+\alpha} k^2 \langle \mathfrak{F}[h], S_R(\theta, \widetilde{\theta}, k) \rangle_{l^2(\mathbb{C})} + O(\varepsilon^*)^2, \tag{3.4}$$

where $P_R(\theta, \widetilde{\theta}, k)$ represents the quantity

$$P_R(\theta, \widetilde{\theta}, k) \quad := \quad J_0(2kR\sin((\widetilde{\theta} - \theta)/2)) - J_2(2kR\sin((\widetilde{\theta} - \theta)/2)) \tag{3.5}$$

and $S_R(\theta, \widetilde{\theta}, k) \in l^2(\mathbb{C})$ is a vector given by

$$S_R(\theta, \widetilde{\theta}, k)_l \quad := \quad i^l e^{-il(\widetilde{\theta}+\theta)/2} J_l(2kR\sin((\widetilde{\theta} - \theta)/2)) \,. \tag{3.6}$$

With the above estimate of the far-field pattern, we can calculate the expression of the magnitude of the far-field pattern, namely $|A_\infty(\theta, \widetilde{\theta}, k)|$, by

$$\frac{|A_\infty(\theta_i, \widetilde{\theta}_i, k_i)|^2 - \pi^2 R^4 (\varepsilon^*)^2 k^4 \left(P_R(\theta_i, \widetilde{\theta}_i, k_i) \right)^2}{4\pi^2 R^3 (\varepsilon^*)^{2+\alpha} k^4 P_R(\theta_i, \widetilde{\theta}_i, k_i)} \quad = \quad \mathrm{Re}\langle \mathfrak{F}[h], S_R(\theta_i, \widetilde{\theta}_i, k_i) \rangle_{l^2(\mathbb{C})} + O(\varepsilon^*)^{1-\alpha}$$

$$= \quad \langle \mathfrak{F}[h], S_R(\theta_i, \widetilde{\theta}_i, k_i) \rangle_{l^2(\mathbb{R}^2)} + O(\varepsilon^*)^{1-\alpha}. \tag{3.7}$$

Due to its great importance for both the subsequent phased and phaseless reconstructions, we state it in the following corollary.

Corollary 3.2. *For $\delta = (\varepsilon^*)^\alpha$ for $0 < \alpha < 1$ it holds that*

$$\langle \mathfrak{F}[h], S_R(\theta_i, \widetilde{\theta}_i, k_i) \rangle_{l^2(\mathbb{R}^2)} = \frac{|A_\infty(\theta_i, \widetilde{\theta}_i, k_i)|^2 - \pi^2 R^4 (\varepsilon^*)^2 k^4 \left(P_R(\theta_i, \widetilde{\theta}_i, k_i) \right)^2}{4\pi^2 R^3 (\varepsilon^*)^{2+\alpha} k^4 P_R(\theta_i, \widetilde{\theta}_i, k_i)} + O(\varepsilon^*)^{1-\alpha}. \tag{3.8}$$

One interesting observation is that $P_R(\theta, \widetilde{\theta}, k)$ and $S_R(\theta, \widetilde{\theta}, k)$ become very simple for $\theta = \widetilde{\theta}$:

$$P_R(\theta, \theta, k) = 1, \quad S_R(\theta, \widetilde{\theta}, k)_l = \delta_{l0}. \tag{3.9}$$

And the expression for the far-field pattern is simplified to

$$A_\infty(\theta, \theta, k) = \pi R^2 \varepsilon^* k^2 + 2\pi R (\varepsilon^*)^{1+\alpha} k^2 \mathfrak{F}[h](0) + O(\varepsilon^*)^2, \tag{3.10}$$

which illustrates that the direct backscattering data $A_\infty(\theta, \theta, k)$ may only provide the information about the area and volume of the inclusions but not the first order perturbation.

We end this section with an important remark about some similarities and differences between the phased and phaseless reconstructions in the linearized case. As we see from (3.4) that

$$\langle \mathfrak{F}[h], S_R(\theta, \widetilde{\theta}, k) \rangle_{l^2(\mathbb{C})} = \frac{A_\infty(\theta_i, \widetilde{\theta}_i, k_i) - \pi R^2 \varepsilon^* k^2 P_R(\theta_i, \widetilde{\theta}_i, k_i)}{2\pi R^2 (\varepsilon^*)^{1+\alpha} k^2} + O(\varepsilon^*)^{1-\alpha}, \tag{3.11}$$

which might be comparable to Corollary 3.2 above. However, we do see several differences here. First, we obtain an approximate value of $\langle \mathfrak{F}[h], S_R(\theta_i, \widetilde{\theta}_i, k_i) \rangle_{l^2(\mathbb{C})}$ with the phased measurements in the linearized case, while an approximate value of $\langle \mathfrak{F}[h], S_R(\theta_i, \widetilde{\theta}_i, k_i) \rangle_{l^2(\mathbb{R}^2)}$ with the phaseless measurements, which is the projection of the original complex inner product to the real part. Therefore, we can regard the linearized phaseless reconstruction as an "half-dimension" analogy of the linearized phased reconstruction. Second, in the phased reconstruction, the denominator of the right hand side of the equation (3.11) does not involve the division of the term $P_R(\theta_i, \widetilde{\theta}_i, k_i)$, whereas in the phaseless reconstruction the division of the term is involved (cf. (3.8)). Both differences make the phaseless reconstruction more ill-posed than the phased one. These differences will be clearly elaborated in section 7.3. As the last point, it is well-known that the phaseless reconstruction is not unique in a sense that any translation of the inclusion yields the same phaseless measurement. But this is not reflected from the above equation, as we have assumed the inclusion is in the center for the sake of exposition.

6

4 A phased reconstruction algorithm in the linearized case

In this section, we provide a reconstruction algorithm for the phased measurement in the linearized case using the concept of the scattering coefficients, and then a resolution analysis of this algorithm.

4.1 An algorithm for phased reconstruction

We recall that ε^* is the contrast of the inclusion D (cf. (1.2)) and the perturbation parameter δ of D is of the order $\delta = (\varepsilon^*)^\alpha$ for $0 < \alpha < 1$. Then motivated by the results in Theorems 2.2 and 2.4, we come to the following reconstruction algorithm in the linearized case.

Algorithm 1. Given the measurement $A_\infty^{\mathrm{meas}}(\theta, \widetilde{\theta}, k)$.

1. Compute W_{nm}^{meas} from the Fourier transform as in (2.9) for $-N < n, m < N$.

2. Find R, ε^* from the following minimization problem

$$\min_{R,\,\varepsilon^*} \sum_{-N<n<N} \left| W_{nn}^{\mathrm{meas}} - \pi R^2 \varepsilon^* k^2 [J_l(kR)^2 - J_{l-1}(kR)J_{l+1}(kR)] \right|^2 . \tag{4.1}$$

3. Compute from (2.14) the estimator $(\delta\, \mathfrak{F}[h])^{est}$ of the product of magnitude δ and Fourier coefficients $\mathfrak{F}[h]$ of the perturbation h for $l \neq 0$:

$$(\delta\, \mathfrak{F}[h])^{est} := \frac{1}{2N-l} \sum_{m-n=l,\, -N<n,m<N} \frac{W_{nm}^{\mathrm{meas}} - W_{nm}(B, \varepsilon^*, k)}{2\pi R \varepsilon^* k^2 J_n(kR) J_m(kR)} . \tag{4.2}$$

We remark that the reconstruction formula (4.2) is similar to the one (5.3) in [5]. Indeed, considering equations (3.26) in [5], with any contrast ε^*, the Fourier coefficients of any perturbation h of $B = B_R(0)$ can always be recovered by an inversion of the operator $A(\varepsilon^*)$ as defined in (4.62) in [5] (after a normalization of its wave number k to $k = 1$). However, the coefficients of the matrix $A(\varepsilon^*)$, i.e. $C(\varepsilon^*, n, m)$ defined in (3.27) in [5], is only given by an expression of resolvent operators, and therefore their explicit expressions are unknown. The inversion formula (5.3) in [5] is hence inconvenient to be used. Nonetheless, for a small contrast ε^*, we know now from Theorem 2.4 an explicit approximation of coefficients $C(\varepsilon^*, n, m)$ as $C(\varepsilon^*, n, m) \approx 2\pi R k^2 (\varepsilon^*)^{1+\alpha} J_n(kR) J_m(kR)$. Therefore (4.2) can be regarded as an easy-to-use approximation of the inversion formula (5.3) of the operator $A(\varepsilon^*)$ described in [5] when the contrast ε^* is small.

4.2 Resolution analysis with respect to signal-to-noise ratio

In this subsection, we perform a resolution analysis of Algorithm 1 in the previous section, which applies also to other reconstruction process derived from (3.11), since the above algorithm is just a Fourier-transformed version of (3.11). Resolution analysis of the above reconstruction with respect to the signal-to-noise ration (SNR) can be conducted following the spirit of the work [7].

In what follows, we assume the following noise model for the far-field pattern:

$$A_\infty^{\mathrm{meas}}(\theta_i, \widetilde{\theta}_j, k) := A_\infty(\theta_i, \widetilde{\theta}_j, k) + N(\theta_i, \widetilde{\theta}_j, k) \tag{4.3}$$

where the pairs $\{(\theta_i, \widetilde{\theta}_i)\}_{i,j=1}^M$ represent the M incident and receiving angles of the measurement evenly distributed on the circle (where M is very large) and $(N(\theta_i, \widetilde{\theta}_j, k))_{i,j=1}^M$ is modeled as, for any fixed value of k, a complex circular symmetric Gaussian white noise vector with variance:

$$\mathbb{E}[|N(\theta_i, \widetilde{\theta}_j, k)|^2] = \sigma^2 k^4 . \tag{4.4}$$

Here σ represents the noise magnitude and the noise term is assumed to have a variance of quadratic growth with respect to k, as it is direct from (2.10) and (2.11) to see that the magnitude of $A_\infty^{\mathrm{meas}}(\theta_i, \widetilde{\theta}_j, k)$ grows in the order of k^2 as k grows.

7

From the well-known fact that any orthogonal transformation of a Gaussian white random vector will result in another Gaussian white random vector, we arrive at, after taking the discrete Fourier transform in the variables θ and $\widetilde{\theta}$, that the following model for the scattering coefficient should be in force:

$$W_{nm}^{\mathrm{meas}}(B^\delta, \varepsilon^*, k) = W_{nm}(B^\delta, \varepsilon^*, k) + \hat{N}_{n,m,\varepsilon^*}, \tag{4.5}$$

where the noise term $\hat{N}_{n,m,\varepsilon^*}$ is another complex circular symmetric Gaussian random variable such that its variance $\mathbb{E}[|\hat{N}_{n,m,\varepsilon^*}|^2]$ (i.e. the power spectrum of the original random variable $N(\theta_i, \widetilde{\theta}_j, k)$) behaves like

$$\mathbb{E}[|\hat{N}_{n,m,\varepsilon^*}|^2] = \sigma^2 k^4. \tag{4.6}$$

Assume a pair of generic (k, R) such that kR is not a zero of J_n for all n. Then for $l \neq 0$, we obtain from a direct subtraction of (2.14) from (4.2), together with (4.5), that

$$\mathfrak{F}[h](l) = (\mathfrak{F}[h])^{est}(l) + \frac{\sigma}{(\varepsilon^*)^{1+\alpha}} N_l + (\varepsilon^*)^{1-\alpha} V_l,$$

where V_l represents the approximation error and N_l a noise term satisfying the following estimate for its variance for a small $R < 1$ and large $N < M$ using (4.6):

$$
\begin{aligned}
\mathbb{E}[|N_l|^2] &= C \frac{1}{(2N-l)^2} \sum_{m-n=l,\, -N<n,m<N} R^{-2}[J_n(kR)J_m(kR)]^{-2} \\
&\leq C \frac{1}{(2N-l)^2 R^2} \sum_{m-n=l,\, -N<n,m<N} \frac{m^m n^n}{R^{2(m+n)}} \\
&\leq C \frac{N^{4N}}{R^{2+4N}}.
\end{aligned} \tag{4.7}
$$

The last second inequality above comes from the asymptotic behavior of the Bessel function [1]:

$$J_n(t) \bigg/ \frac{1}{\sqrt{2\pi|n|}} \left(\frac{et}{2|n|}\right)^{|n|} \to 1 \tag{4.8}$$

as $|n| \to \infty$. Now assume further that $\varepsilon^* << \sqrt{\sigma}$ and

$$\mathrm{SNR} := \left(\frac{\varepsilon^*}{\sigma}\right)^2,$$

then we get

$$\mathbb{E}[|(\mathfrak{F}[h])^{est}(l)|] = \mathfrak{F}[h](l), \quad \mathbb{E}[|(\mathfrak{F}[h])^{est}(l) - \mathfrak{F}[h](l)|^2] \leq C \frac{N^{4N}}{R^{2+4N}} (\mathrm{SNR})^{-(1+\alpha/2)}, \tag{4.9}$$

which enables us to conclude the following result.

Theorem 4.1. *Suppose that $\delta = (\varepsilon^*)^\alpha$ for $0 < \alpha < 1$, and $M >> 1$ is the number of measurement points. If $N < M$ is selected such that*

$$C \frac{N^{4N}}{R^{2+4N}} < (SNR)^{1+\alpha/2} \tag{4.10}$$

and that $\mathfrak{F}[h](l)$ ($|l| \leq N$) are of order 1, then the l-th mode of h can be resolved for $|l| \leq N$, i.e. $\mathbb{E}[|(\mathfrak{F}[h])^{est}(l) - \mathfrak{F}[h](l)|^2] < 1$.

5   Introduction to phaseless reconstruction

Phaseless reconstruction originates from the physical background that we can usually only measure the magnitude of some data, for example, the magnitude of the far-field pattern. As briefly explained in section 1, it is quite difficult and expensive to obtain the phased data in many physical and engineering applications, and the phase of a measurement is easily contaminated by noise. On the other hand, the phaseless data is much easier to obtain and less contaminated in many practical situations. Due to these facts, the phaseless reconstruction has attracted wide attention.

5.1 Brief history of a general phaseless reconstruction problem

Let us first give a brief introduction and history of a general phaseless reconstruction. As in [12], for a given set of m sampling vectors, $\mathbf{z}_1, \cdots, \mathbf{z}_m$, we intend to recover a vector $\mathbf{x}$ from some phaseless data. This may be formulated as

$$\text{Find } \mathbf{x} \text{ such that } A(\mathbf{x}) = b \tag{5.1}$$

where $A : \mathbb{C}^N \to R^m$ is given by $A(\mathbf{x})_i = |\langle \mathbf{x}, \mathbf{z}_i \rangle|^2$. One may consider a convexification of the problem (5.1) [12]:

$$\text{Find } \mathbf{X} \geq 0 \text{ such that } \mathcal{A}(\mathbf{X}) = b, \tag{5.2}$$

where $\mathcal{A} : \mathcal{H}^{N \times N} \to R^m$ is given by $\mathcal{A}(\mathbf{X}) = \mathbf{z}_i^* \mathbf{X} \mathbf{z}_i$, which helps reduce the complexity of solving the problem, as well as provide uniqueness results under some practical conditions. For instance, this problem is proven to have a high probability that it is uniquely solvable up to a unit complex number stably from $O(N \log N)$ random measurements [21]. We remark that a stablized version of convexification is given by

$$\text{Find } \mathbf{X} \geq 0 \text{ such that } ||\mathcal{A}(\mathbf{X}) - b|| \leq \epsilon ||X_0||_2. \tag{5.3}$$

Another more general form of phaseless reconstruction (which generalizes the above) comes from recovering the phase of a function/vector from the modulus of its evaluation by a family of functionals. In a more precise way, let E be a complex vector space and $\{L_i\}_{i \in I}$ be a family of functionals. Then this phaseless reconstruction reads:

$$\text{Find } \mathbf{f} \in E \text{ such that } |L_i(\mathbf{f})| = b. \tag{5.4}$$

In the case where $\{L_i\}_{i \in I}$ represents the wavelet transform by the Cauchy wavelets, it was shown in [38] that the modulus of the wavelet transform uniquely determines the function up to a global phase, and the reconstruction operator is continuous but not uniformly continuous.

5.2 Introduction to our phaseless reconstruction problem

The convexification discussed in section 5.1 is a very interesting approach, but the purpose, framework and analysis of our phaseless reconstruction here are very different. We aim to achieve numerical reconstructions of inhomogeneous domains in the linearized case. We will provide an algorithm for the domain reconstruction from some phaseless far-field data, and estimate the condition number of this reconstruction process, and establish an upper bound of its infimum over all phaseless measurement strategies. This casts light on how we can obtain an optimal strategy to perform effective phaseless measurements such that the phaseless inversion process shall be well-posed. For comparison purpose, a similar analysis technique is also performed on its phased counterpart, and a comparison between the phased and phaseless reconstructions shall be made.

6 Phaseless domain reconstruction algorithm in linearized cases

In this section, we provide a new method for the domain reconstruction from the phaseless far-field data based on our analyses and results in sections 2 and 3. We first recall from Theorem 3.2 the relation

$$\frac{|A_\infty(\theta_i, \widetilde{\theta}_i, k_i)|^2 - \pi^2 R^4 (\varepsilon^*)^2 k^4 \left(P_R(\theta_i, \widetilde{\theta}_i, k_i)\right)^2}{4\pi^2 R^3 (\varepsilon^*)^{2+\alpha} k^4 P_R(\theta_i, \widetilde{\theta}_i, k_i)} = \langle \mathfrak{F}[h], S_R(\theta_i, \widetilde{\theta}_i, k_i) \rangle_{l^2(\mathbb{R}^2)} + O(\varepsilon^*)^{1-\alpha}, \tag{6.1}$$

where $P_R(\theta_i, \widetilde{\theta}_i, k_i) \in \mathbb{R}$ and $S_R(\theta_i, \widetilde{\theta}_i, k_i) \in l^2(\mathbb{C})$ are given in (3.5) and (3.6). Therefore, from a finite number of M measurements $|A_\infty(\theta_i, \widetilde{\theta}_i, k_i)|$ ($1 \leq i \leq M$), we obtain the following linear approximation of $\langle \mathfrak{F}[h], S_R(\theta_i, \widetilde{\theta}_i, k_i) \rangle$ as the measurement quantities from the phaseless measurements:

$$\langle \mathfrak{F}[h], S_R(\theta_i, \widetilde{\theta}_i, k_i) \rangle_{l^2(\mathbb{R}^2)} \approx \frac{|A_\infty(\theta_i, \widetilde{\theta}_i, k_i)|^2 - \pi^2 R^4 (\varepsilon^*)^2 k^4 |P_R(\theta_i, \widetilde{\theta}_i, k_i)|^2}{4\pi^2 R^3 (\varepsilon^*)^{2+\alpha} k^4 P_R(\theta_i, \widetilde{\theta}_i, k_i)}. \tag{6.2}$$

This is of crucial importance for us to derive an algorithm for the domain reconstruction from the phaseless far-field measurements.

6.1 Phaseless reconstruction algorithm

We are now ready to introduce our phaseless reconstruction algorithm. Following Theorem 4.1 from the resolution analysis for the phased reconstruction in section 3, we can directly infer that the resolution with respect to SNR in the phaseless reconstruction should not surpass the N-th Fourier mode, where N satisfies the inequality $C\frac{N^{4N}}{R^{2+4N}} < (\mathrm{SNR})^{1+\alpha/2}$ for some C and α. Hence in our reconstruction algorithm, we may always assume that $\mathfrak{F}[h](l) = 0$ for $|l| > N$ for some N and consider only the inversion of finite dimensional operators, and the contribution of $\mathfrak{F}[h](l)$ for $|l| > N$ to the measurement data can be regarded as noise. Now since $h(\theta) \in \mathbb{R}$ for all θ, we have the following additional constraints on the Fourier coefficients:

$$\mathfrak{F}[h](-l) = \overline{\mathfrak{F}[h](l)}. \tag{6.3}$$

This set of constraints is very important in our subsequent analysis. We assume again that the magnitude of the perturbation δ is of the form $\delta = (\varepsilon^*)^\alpha$ for $0 < \alpha < 1$, where ε^* is the contrast of the inclusion. From Theorem 3.2, we can now suggest the following phaseless reconstruction algorithm.

Algorithm 2. Given a positive integer N and M measurements of the magnitude $|A_\infty^{\mathrm{meas}}(\theta_i, \widetilde{\theta}_i, k_i)|$ $(1 \leq i \leq M)$ of the far-field.

1. Find the pair (R, ε^*) that minimizes the following functional:

$$\sum_{1 \leq i \leq M} \left| |A_\infty^{\mathrm{meas}}(\theta_i, \widetilde{\theta}_i, k_i)|^2 - \pi^2 R^4 k^4 \varepsilon^{*2} \left(P_R(\theta_i, \widetilde{\theta}_i, k_i) \right)^2 \right|^2, \tag{6.4}$$

   where the values $P_R(\theta_i, \widetilde{\theta}_i, k_i)$ are computed from (3.5).

2. Compute the following quantities for $1 \leq i \leq M$:

$$\frac{|A_\infty^{\mathrm{meas}}(\theta_i, \widetilde{\theta}_i, k_i)|^2 - \pi^2 R^4 \varepsilon^{*2} k^4 |P_R(\theta_i, \widetilde{\theta}_i, k_i)|^2}{4\pi^2 R^3 \varepsilon^{*2} k^4 P_R(\theta_i, \widetilde{\theta}_i, k_i)}. \tag{6.5}$$

3. Calculate the estimator $(\delta\,\mathfrak{F}[h])^{est}(l)$ of the product of magnitude δ and Fourier coefficient $\mathfrak{F}[h]$ of the perturbation h for $|l| \leq N$ by the inversion of the following system of linear equations:

$$\langle (\delta\,\mathfrak{F}[h])^{est}, S_R(\theta_i, \widetilde{\theta}_i, k_i) \rangle_{l^2(\mathbb{R}^2)} = \frac{|A_\infty^{\mathrm{meas}}(\theta_i, \widetilde{\theta}_i, k_i)|^2 - \pi^2 R^4 \varepsilon^{*2} k^4 |P_R(\theta_i, \widetilde{\theta}_i, k_i)|^2}{4\pi^2 R^3 \varepsilon^{*2} k^4 P_R(\theta_i, \widetilde{\theta}_i, k_i)}, \tag{6.6}$$

   under the constraints

$$(\mathfrak{F}[h])^{est}(-l) = \overline{(\mathfrak{F}[h])^{est}(l)}. \tag{6.7}$$

We should be reminded that the above algorithm can only provide stable inversion and reasonable resolution of the perturbation h up to at most the N-th Fourier mode, where N shall satisfy the inequality $C\frac{N^{4N}}{R^{2+4N}} < (\mathrm{SNR})^{1+\alpha/2}$ for some C and α, as shown in Theorem 4.1 in section 3.

7 Stability of the phaseless domain reconstruction

We are now ready to discuss the stability of the phaseless reconstruction by estimating the condition number of this inversion process. Before going into detailed estimates, we shall state our inversion problem in a more concise manner, which will provide a clear framework for our subsequent analysis. For this purpose, we first define three operators for a given pair $(N, M) \in \mathbb{N}$, where two of them are linear in nature while the other one is nonlinear:

1. the component-wise squaring of a vector followed by a subtraction of another known vector, i.e. the action $v_i \mapsto v_i^2 - \pi^2 R^4 \varepsilon^{*2} k^4 |P_R(\theta_i, \widetilde{\theta}_i, k_i)|^2$, which appears in Step 2 of Algorithm 2; and we write this nonlinear operator as $F : \mathbb{R}^M \to \mathbb{R}^M$;

10

2. the component-wise multiplication of a vector $v_i \mapsto 4\pi^2 R^3 \varepsilon^{*2} k^4 P_R(\theta_i, \widetilde{\theta}_i, k_i) \, v_i$, which appears in Step 2 of Algorithm 2; and we will write this linear operator as $L : \mathbb{R}^M \to \mathbb{R}^M$;

3. the linear operator $v \mapsto \left(\langle v, S_R(\theta_i, \widetilde{\theta}_i, k_i) \rangle_{l^2(\mathbb{R}^2)} \right)_{i=1}^M$, which appears in Step 3 of Algorithm 2. We shall write this linear operator as $T : \mathbb{C}^{2N} \oplus \{0\} \cong \mathbb{R}^{4N} \to \mathbb{R}^M$.

Without loss of generality, we may always choose a radius R such that the zeroth Fourier coefficient $\mathfrak{F}[h](0)$ is zero. With these preparations, we can write (6.6) as

$$(L \circ T) \left[(\delta \, \mathfrak{F}[h])^{est} \right] = F(|A_\infty^{\mathrm{meas}}(\theta_i, \widetilde{\theta}_i, k_i)|) \,. \tag{7.1}$$

Then our phaseless inversion problem can be precisely stated as follows: given a value of SNR, with a number N such that $CN^{4N}/R^{2+4N} < (\mathrm{SNR})^{1+\alpha/2}$ for some C and α, we recover the Fourier coefficients $\delta \left(\mathfrak{F}[h]^{est}(l) \right)_{l=-N}^N \in \mathbb{C}^{2N} \oplus \{0\} \cong \mathbb{R}^{4N}$ from (7.1) with M measurements:

$$(b_i)_{i=1}^M := F(|A_\infty^{\mathrm{meas}}(\theta_i, \widetilde{\theta}_i, k_i)|) = \left(|A_\infty^{\mathrm{meas}}(\theta_i, \widetilde{\theta}_i, k_i)|^2 - \pi^2 R^4 \varepsilon^{*2} k^4 |P_R(\theta_i, \widetilde{\theta}_i, k_i)|^2 \right)_{i=1}^M \in \mathbb{R}^M$$

subjected to the following extra set of constraints in $\mathbb{R}^{4N}$ as

$$\mathrm{Re}(\mathfrak{F}[h])^{est}(-l) - \mathrm{Re}(\mathfrak{F}[h])^{est}(l) = 0 \,, \qquad \mathrm{Im}(\mathfrak{F}[h])^{est}(-l) + \mathrm{Im}(\mathfrak{F}[h])^{est}(l) = 0 \,.$$

From now on, we shall denote this set of linear constraints as

$$C \left[(\delta \, \mathfrak{F}[h])^{est} \right] = 0 \,. \tag{7.2}$$

After this restatement of the phaseless reconstruction problem, we can directly infer that the stability of the inversion lies in the stability of inversion of the linear operators L and T in the subspace $\ker(C)$ under a certain noise level. Therefore, the aim of this section is to estimate the condition numbers of the operators T and L in this subspace. To the best of our knowledge, the stability estimates on condition numbers are novel for inverse problems, and are very important for us to understand the degree of ill-posedness and stability of the reconstruction problem, as well as to provide optimal methods to minimize these two condition numbers by making wise measurements or regularizations.

7.1 Estimation of the condition number of T

We come now to the estimate of the condition number of operator T. For notational sake, we first introduce two more operators, $\iota_0 : \mathbb{C} \to \mathbb{R}^2 \,, z \mapsto (\mathrm{Re}(z), \mathrm{Im}(z))$ and their liftings on the linear operators over the corresponding spaces $\iota : \mathfrak{L}(\mathbb{C}) \cong \mathbb{C} \to \mathfrak{L}(\mathbb{R}^2) \cong M_{2 \times 2} \,, z \mapsto \begin{pmatrix} \mathrm{Re}(z) & \mathrm{Im}(z) \\ -\mathrm{Im}(z) & \mathrm{Re}(z) \end{pmatrix}$. And we shall also use the projection map $\pi_{\mathrm{Re}} : M_{2 \times 2} \to M_{1 \times 2} \,, \begin{pmatrix} a & b \\ c & d \end{pmatrix} \mapsto \begin{pmatrix} a & b \end{pmatrix}$. It is easy to check

$$[\pi_{\mathrm{Re}} \circ \iota(\bar{z})] (\iota_0(w)) = \langle \iota_0(z), \iota_0(w) \rangle_{\mathbb{R}^2} = \mathrm{Re}(\bar{z}w) \,. \tag{7.3}$$

Before we go on to study the stability of the reconstruction problem, we shall also provide a clear concept and define the condition number of T subjected to the constraint $Cx = 0$, denoted as $\kappa(T, \ker(C))$, where $C : \mathbb{R}^P \to \mathbb{R}^Q$ for $Q \leq P$ is another linear operator. First, for the sake of exposition, we shall denote $C^\perp$ as the set of all matrices E such that its column vectors are linearly independent and span the orthogonal complement of the row space of $C = (C_1, C_2, \dots, C_n)^T$, i.e.

$$C^\perp := \{ (E_1, E_2, \dots, E_n) : \langle E_1, \dots, E_n, C_1, \dots, C_n \rangle = \mathbb{R}^P, \langle E_1, \dots, E_{j-1}, E_{j+1}, \dots, E_n, C_1, \dots, C_n \rangle \neq \mathbb{R}^P \;\; \forall j \} \,.$$

Now, if we solve the following constraint problem for a given triple (T, b, C):

$$\text{Find } x \in \mathbb{R}^P \text{ such that } \quad Tx = b \quad \text{and} \quad Cx = 0 \,,$$

or its least-squares formulation:

$$\min_{\substack{x \in \mathbb{R}^P \\ s.t. \ Cx=0}} ||Tx - b||_2^2 \,,$$

we are actually parameterizing the kernel $\ker(C)$ by an orthogonal complement of the row space of C, and then solve the equation $Tx = b$ under this parametrization (either in the strict sense, or the least-squares sense), i.e., solve for y the equation (with $E \in C^{\perp}$):

$$(T \circ E)\, y = b \,,$$

or the least-squares minimization (with $E \in C^{\perp}$):

$$\min_{y \in \mathbb{R}^Q} ||(T \circ E)\, y - b||_2^2 \,.$$

From this definition, one can easily get that the operator T is invertible with its solution in the subspace $Cx = 0$ if and only if $T \circ E$ is invertible. One can also directly get that if $Tx = b$ and $T\tilde{x} = \tilde{b}$ where $x, \tilde{x} \in \ker C$, then we have the following estimate

$$\frac{||y - \tilde{y}||}{||y||} \leq \kappa(T \circ E)\frac{||b - \tilde{b}||}{||b||} \,,$$

for any $E \in C^{\perp}$, where $y, \tilde{y}$ are defined such that $Ey = x, E\tilde{y} = \tilde{x}$. Hence, in order to study the stability of the inversion process of T in the subspace, we are motivated to define the condition number of T under the constraint $Cx = 0$ as

$$\kappa(T, \ker(C)) := \inf\{\kappa(T \circ E) \ : \ E \in C^{\perp}\} \,. \tag{7.4}$$

7.1.1 A measurement strategy for phaseless reconstruction

In this subsection, we proceed to develop a good measurement strategy which can minimize the condition number of T and ensure the well-posedness of the inversion concerned.

Indeed, we shall intuitively expect to have a good strategy in choosing the measurement set $(\theta, \widetilde{\theta}, k)$ by gazing at the vector S_R in (3.6): for a given target resolution N, one may choose $2k_i R \sin((\widetilde{\theta}_i - \theta_i)/2)$ such that they attain the m_0-th local extremum of J_l for $1 < l < N$, i.e., the values of b_{l,m_0} where $J_l'(b_{l,m_0}) = 0$ for a given m_0. With this particular choice of M sets of measurement data $\{(\theta_i, \widetilde{\theta}_i, k_i)\}_{i=1}^M$ such that $2k_i R \sin((\widetilde{\theta}_i - \theta_i)/2) \in \{b_{1,m_0}, b_{2,m_0}, ..., b_{N,m_0}\}$, the operator T is expected to be well-conditioned and therefore provide a good set of information for the geometry of the inclusion. This shall be indeed verified in this subsection.

In what follows, we aim to estimate, for a given resolution N, the infimum over the condition numbers of all the operators $T : \mathbb{R}^{4N} \to \mathbb{R}^M$ subjected to the constraint $Cx = 0$, i.e.,

$$\kappa_{\inf, N} := \inf\left\{\kappa(T, \ker(C)) \ : \ \{(\theta_i, \widetilde{\theta}_i, k_i)\}_{i=1}^M \in [0.2\pi]^2 \times (0, \infty)\,, \ M \in \mathbb{Z}\right\}$$

by appropriately choosing the vectors $\{(\theta_i, \widetilde{\theta}_i, k_i)\}_{i=1}^M$. Indeed, from the following well-known asymptotic of J_l [1] for all l:

$$J_l(z) = \sqrt{\frac{2}{\pi z}} \cos\left(z - \frac{2l+1}{4}\pi\right) + O(z^{-3/2}) \,, \tag{7.5}$$

we directly have for a fixed l that

$$b_{l,m_0} \bigg/ \frac{(4m_0 + 2l + 1)\pi}{4} \to 1 \tag{7.6}$$

12

as m_0 goes to infinity. Therefore, for a given large m_0, if we choose $(\theta_i, \widetilde{\theta}_i, k_i)$ as the form $(\theta_i, \theta_i + \pi, \frac{4m_0 + 2J_i + 1}{8R})$, where $(J_i)_{i=1}^{M} \in \mathbb{Z}$ are some integral indices to be specified later, then we have directly from (7.5) and (7.6) that

$$S_R(\theta_i, \widetilde{\theta}_i, k_i)_l = e^{il\theta_i} \sqrt{\frac{16R}{\pi(4m_0 + 2J_i + 1)}} \cos\left(\left(m_0 + \frac{J_i - l}{2}\right)\pi\right) + O(m_0^{-3/2}). \tag{7.7}$$

Let T_{m_0} be the linear operator T with this specific arrangement of measurements for a given m_0. If we further denote $L := T_{m_0}^T T_{m_0}$ in the form of a block matrix $(L_{lm})_{-N \leq l,m \leq N, l,m \neq 0}$, then from (7.3), each of the block L_{lm} will be the following 2×2 matrix:

$$
\begin{aligned}
L_{lm} &= \iota_0 \left[S_R(\theta_i, \widetilde{\theta}_i, k_i)_l \right]^T \iota_0 \left[S_R(\theta_i, \widetilde{\theta}_i, k_i)_m \right] \\
&= \frac{16R}{\pi} \iota \left[\sum_{i=1}^{M} L_{l,m,\theta_i} \frac{1}{4m_0 + 2J_i + 1} \cos\left(\left(m_0 + \frac{J_i - m}{2}\right)\pi\right) \cos\left(\left(m_0 + \frac{J_i - l}{2}\right)\pi\right) \right] + O(m_0^{-2}),
\end{aligned}
$$

where the matrix $L_{l,m,\theta}$ has the form

$$L_{l,m,\theta} = \begin{pmatrix} \cos(m\theta)\cos(l\theta) & \cos(m\theta)\sin(l\theta) \\ \cos(m\theta)\sin(l\theta) & \sin(m\theta)\sin(l\theta) \end{pmatrix}.$$

For the sake of exposition, we further denote $\theta_i = 2\pi I_i / N$ where $(I_i)_{i=1}^{M} \in \mathbb{Z}$ are some indices to be chosen later.

We are now ready to specify our choice of indices $\{(I_i, J_i)\}_{i=1}^{M}$. In particular we let the array $\{(I_i, J_i)\}_{i=1}^{M}$ be such that it enumerate the index set $\{(I, J) : 1 \leq I \leq N, 1 \leq J \leq N\}$, i.e., we have $M = N^2$. With the above definition, we readily see

$$
\begin{aligned}
&L_{lm} \\
&= \frac{16R}{\pi} \sum_{J=1}^{N} \left[\sum_{I=1}^{N} L_{l,m,\frac{2\pi I}{N}} \right] \frac{1}{4m_0 + 2J + 1} \cos\left(\left(m_0 + \frac{J-m}{2}\right)\pi\right) \cos\left(\left(m_0 + \frac{J-l}{2}\right)\pi\right) + O(m_0^{-2}) \\
&= \frac{16RN}{\pi} \delta_{|l|,|m|} \begin{pmatrix} 1 & 0 \\ 0 & \operatorname{sgn}(l)\operatorname{sgn}(m) \end{pmatrix} \sum_{J=1}^{N} \frac{1}{4m_0 + 2J + 1} \cos^2\left(\frac{(J-m)\pi}{2}\right) + O(m_0^{-2}),
\end{aligned}
$$

where $\delta_{a,b}$ is the kronecker delta for any $a, b \in \mathbb{N}$.

From the above summation, we can directly infer that

$$L_{lm} = \frac{16RN}{\pi} \delta_{|l|,|m|} \begin{pmatrix} 1 & 0 \\ 0 & \operatorname{sgn}(l)\operatorname{sgn}(m) \end{pmatrix} \sum_{J=0}^{\left[\frac{N-1}{2}\right]} \frac{1}{4m_0 + 4J + 2\operatorname{mod}_2(m) + 1} + O(m_0^{-2}), \tag{7.8}$$

where mod_2 is the standard mod-2 function and $[\cdot]$ is the floor function. Now, for the sake of exposition, we denote for given $C, m_0, \widetilde{M}$ a coefficient $K_{C,m_0,\widetilde{M}}$ as

$$K_{C,m_0,\widetilde{M}} := \sum_{J=1}^{\widetilde{M}} \frac{1}{4m_0 + 1 + 4J + 2C}. \tag{7.9}$$

With this definition, we now hope to approximate $K_{C,m_0,\widetilde{M}}$. In fact, from the comparison test, we directly arrive at, for any fixed $m_0, \tilde{M}$ and any $C = 0, 1$, that the following holds:

$$\frac{1}{4} \log\left(1 + \frac{\tilde{M}}{m_0 + 2}\right) \leq K_{C,m_0,\tilde{M}} \leq \frac{1}{4} \log\left(1 + \frac{\tilde{M}}{m_0 + 1}\right). \tag{7.10}$$

Then we can write

$$L_{lm} = \frac{16RN}{\pi} \delta_{|l|,|m|} K_{\operatorname{mod}_2(m),m_0,\left[\frac{N-1}{2}\right]} \begin{pmatrix} 1 & 0 \\ 0 & \operatorname{sgn}(l)\operatorname{sgn}(m) \end{pmatrix} + O(m_0^{-2}), \tag{7.11}$$

13

with $K_{\text{mod}_2(m),m_0,[\frac{N-1}{2}]}$ satisfying estimate (7.10). We may now observe a seemingly pathological situation: the matrix L is actually not invertible in $\mathbb{R}^{4N}$. However, this is actually not as pathological as we think it is, because the constraint $Cx = 0$ shall come in to play a fundamental role. To proceed, we can take a matrix $E \in C^\perp$ in the block form $(E_{lm})_{-N \leq l \leq N, l \neq 0, 1 \leq m \leq N}$, as follows:

$$E_{lm} = \delta_{|l|,m} \begin{pmatrix} 1 & 0 \\ 0 & \text{sgn}(l) \end{pmatrix}. \tag{7.12}$$

One easily check that the above block matrix E is indeed in $C^\perp$. Then one directly calculate that, for all $1 \leq l, m \leq N$,

$$\left(E^T \circ L \circ E\right)_{lm} = \frac{64RN}{\pi} \delta_{l,m} K_{\text{mod}_2(m),m_0,[\frac{N-1}{2}]} \begin{pmatrix} 1 & 0 \\ 0 & 1 \end{pmatrix} + O(m_0^{-2}), \tag{7.13}$$

which is now invertible. Hence for a fixed N and the choice $(\theta_i, \widetilde{\theta}_i, k_i)$ of the form $(2\pi I_i/N, 2\pi I_i/N + \pi, \frac{4m_0 + 2J_i + 1}{8R})$, where $\{(I_i, J_i)\}_{i=1}^M$ enumerates through $\{(I, J) : 1 \leq I \leq N, 1 \leq J \leq N\}$, we can directly derive the following estimate for the singular values of T_{m_0}:

$$\frac{4\sqrt{RN}}{\sqrt{\pi}} \sqrt{\log\left(1 + \frac{[\frac{N-1}{2}]}{m_0 + 2}\right)} - \frac{C_N}{m_0^2} \leq s_{\min}(T_{m_0} \circ E) \leq s_{\max}(T_{m_0} \circ E) \leq \frac{4\sqrt{RN}}{\sqrt{\pi}} \sqrt{\log\left(1 + \frac{[\frac{N-1}{2}]}{m_0 + 1}\right)} + \frac{C_N}{m_0^2}$$

where C_N is a constant only depending on N. Therefore, if we write s_{max} and s_{min} respectively as the largest and smallest singular values, then it follows that

$$\kappa(T_{m_0} \circ E) = \frac{s_{\max}(T_{m_0} \circ E)}{s_{\min}(T_{m_0} \circ E)} \leq \sqrt{\log\left(1 + \frac{[\frac{N-1}{2}]}{m_0 + 1}\right) \bigg/ \log\left(1 + \frac{[\frac{N-1}{2}]}{m_0 + 2}\right)} + O(m_0^{-2}). \tag{7.14}$$

The Taylor series of $\log(1 + x)$ and $\sqrt{a + x}$ then give rise to the following estimate for large m_0 that

$$\kappa_{\text{inf},N} \leq \kappa(T_{m_0}, \ker(C)) \leq \kappa(T_{m_0} \circ E) \leq \sqrt{\frac{m_0 + 2}{m_0 + 1}} + O(m_0^{-2}) \leq 1 + O(m_0^{-1}), \tag{7.15}$$

where we should remind ourselves that the big-O terms are bounded by a constant only depending on N. Since m_0 is arbitrary, we get for any given N that the infimum of the condition number $\kappa(T, \ker(C))$ is given by $\kappa_{\text{inf},N} = 1$, and a minimizing sequence to attain this infimum can be actualized by measurements $(\theta_i, \widetilde{\theta}_i, k_i)$ as previously specified as m_0 goes to infinity. This implies that we can always make an appropriate choice of the target resolution N such that the inversion process of T is well-posed. The above analysis can be summarized into the following theorem.

Theorem 7.1. *For a given target resolution N, the infimum $\kappa_{inf,N}$ of the condition number $\kappa(T, \ker(C))$ defined as in (7.5) over the set of linear operators T is given by*

$$\kappa_{inf,N} = 1. \tag{7.16}$$

A minimizing sequence $\kappa(T_{m_0}, \ker(C)), m_0 \in \mathbb{Z}$ of this infimum acquires the following bound

$$\kappa(T_{m_0}, \ker(C)) \leq 1 + O(m_0^{-1}) \tag{7.17}$$

if we make the arrangement of phaseless measurements in the way that the following equality holds:

$$(\theta_i, \widetilde{\theta}_i, k_i) = \left(2\pi I_i/N, 2\pi I_i/N + \pi, \frac{4m_0 + 2J_i + 1}{8R}\right), \tag{7.18}$$

where $\{(I_i, J_i)\}_{i=1}^M$ enumerates through $\{(I, J) : 1 \leq I \leq N, 1 \leq J \leq N\}$ and m_0 is large, hence N^2 phaseless measurements shall be made.

This theorem gives us a very effective strategy of data measurement such that the phaseless reconstruction process shall be well-posed. In particular, an increase of m_0 in the aforementioned measurement method reduces the condition number of the inversion process with an order of $O(m_0^{-1})$ according to (7.17).

7.2 Estimation of the condition number of L

From the previous analysis, we can see that the inversion process of T can be made impressively stable and one can suppress its condition number appropriately. However this does not ensure a very stable phaseless inversion process, owing to the fact from (7.1) that the total inversion process is given by $T^{-1} \circ L^{-1}$.

Although the action of L is simple and explicit, the inversion process may not be as simple as one might think. The condition number of L can be directly calculated as $\max_i |P_R(\theta_i, \widetilde{\theta}_i, k_i)| / \min_i |P_R(\theta_i, \widetilde{\theta}_i, k_i)|$. Therefore the inversion process becomes severely ill-posed when some measurement data has a very small value $|P_R(\theta_i, \widetilde{\theta}_i, k_i)|$, which in turn pushes up the condition number to an arbitrary magnitude. This causes the reconstruction process to be very unstable in practice.

However, a very simple regularization technique can get rid of this instability. Thanks to the fact that $P_R(\theta, \widetilde{\theta}, k)$ is analytic, its value cannot be zero on an open neighborhood, and therefore a simple regularization can be performed on the inversion of L by the operator L_α^{-1} defined as follows:

$$L_\alpha^{-1} = \mathrm{diag}\Big(\chi_{x > \alpha}(|P_R(\theta_i, \widetilde{\theta}_i, k_i)|)[P_R(\theta_i, \widetilde{\theta}_i, k_i)]^{-1} + \alpha^{-1} \chi_{x \le \alpha}(|P_R(\theta_i, \widetilde{\theta}_i, k_i)|) \lim_{(\theta, \widetilde{\theta}, k) \to (\theta_i, \widetilde{\theta}_i, k_i)} \frac{P_R(\theta, \widetilde{\theta}, k)}{|P_R(\theta, \widetilde{\theta}, k)|} \Big) \quad (7.19)$$

where $\chi_{x > \alpha}$ and $\chi_{x \le \alpha}$ are the respective characteristic functions on the intervals $\{x > \alpha\}$ and $\{x \le \alpha\}$. With this definition, we come readily to the following simple but important lemma.

Lemma 7.2. Let L_α^{-1} be defined as in (7.19), then we have

$$\kappa(L^{-1}) = \frac{\max_i |P_R(\theta_i, \widetilde{\theta}_i, k_i)|}{\min_i |P_R(\theta_i, \widetilde{\theta}_i, k_i)|}, \quad \kappa(L_\alpha^{-1}) \le \frac{2}{\alpha}. \quad (7.20)$$

We can see from above that $\kappa(L^{-1})$ cannot be controlled but $\kappa(L_\alpha^{-1})$ has an upper bound, therefore it provides a stable inversion process if α is appropriately chosen.

From (7.1), a stable shape reconstruction process is therefore provided by $T^{-1} \circ L_\alpha^{-1}$. Indeed, the stability estimates (7.17) and (7.20) for the condition numbers of T^{-1} and L_α^{-1} subjected to $Cx = 0$ ensure us the stability of this reconstruction method and provide us optimal strategies to lower the degree of ill-posedness for the phaseless reconstruction problem under the corresponding measurement cases. The stability of our proposed method will be verified in the numerical experiments. To the best of our knowledge, these estimates of condition numbers are completely new to our inverse problems.

7.3 A comparison with the phased reconstruction

As we have remarked in section 3, together with the fact that any translation of the inclusion yields the same phaseless measurement, the phaseless reconstruction is not unique in this sense. And the linearized phased and phaseless reconstructions share some fundamental differences. From (3.11) or its Fourier-transformed version (Algorithm 1), we see that any algorithm derived from (3.11) for the phased reconstruction is equivalent to solving $\delta \left(\mathfrak{F}[h]^{est}(l) \right)_{l=-N}^{N} \in \mathbb{C}^{2N} \oplus \{0\} \cong \mathbb{R}^{4N}$ such that

$$\tilde{T}\left[(\delta \, \mathfrak{F}[h])^{est} \right] = G(A_\infty^{\mathrm{meas}}(\theta_i, \widetilde{\theta}_i, k_i)), \quad (7.21)$$

where N satisfies

$$C \frac{N^{4N}}{R^{2+4N}} < (\mathrm{SNR})^{1+\alpha/2}$$

for some C and α, and $(\mathfrak{F}[h])^{est}$ is again subjected to the constraints

$$\mathrm{Re}(\mathfrak{F}[h])^{est}(-l) - \mathrm{Re}(\mathfrak{F}[h])^{est}(l) = 0, \quad \mathrm{Im}(\mathfrak{F}[h])^{est}(-l) + \mathrm{Im}(\mathfrak{F}[h])^{est}(l) = 0.$$

The operators G and $\tilde{T}$ above are respectively given by

1. $G : \mathbb{C}^M \to \mathbb{C}^M$, the component-wise affine map of a vector, i.e. the action $v_i \mapsto \frac{v_i - \pi R^2 \varepsilon^* k^2 P_R(\theta_i, \widetilde{\theta}_i, k_i)}{2\pi R^2 \varepsilon^* k^2}$.

2. $\tilde{T} : \mathbb{C}^{2N} \to \mathbb{C}^M$, the linear operator $v \mapsto \left(\langle v, S_R(\theta_i, \widetilde{\theta}_i, k_i) \rangle_{l^2(\mathbb{C})} \right)_{i=1}^M$.

A similar stability analysis for the operator $\tilde{T}$ induced by the phased measurements can be performed to the one for the operator $\hat{T}$ corresponding to the phaseless reconstruction as in section 7.1.1. Since most of the steps are similar to the previous analysis for the phaseless reconstruction, we only provide a sketch of the argument. Again we choose $(\theta_i, \widetilde{\theta}_i, k_i)$ of the form $(2\pi I_i/N, 2\pi I_i/N + \pi, \frac{4m_0 + 2J_i + 1}{8R})$ where $\{(I_i, J_i)\}_{i=1}^M \in \mathbb{Z}$ are some integral indices to be specified and let $\tilde{T}_{m_0}$ be the linear operator $\tilde{T}$ with this specific arrangement of measurement with a given m_0. Denoting $\tilde{L} := \iota[\tilde{T}_{m_0}^*] \iota[\tilde{T}_{m_0}]$, then a similar argument, along with the fact that ι is an algebra homomorphism, shows for $-N \leq l, m \leq N$ that

$$\tilde{L}_{lm} = \frac{16R}{\pi} \iota \left[\sum_{i=1}^M \tilde{L}_{l,m,\theta_i} \frac{1}{4m_0 + 2J_i + 1} \cos \left(\left(m_0 + \frac{J_i - m}{2} \right) \pi \right) \cos \left(\left(m_0 + \frac{J_i - l}{2} \right) \pi \right) \right] + O(m_0^{-2}),$$

where each $\tilde{L}_{l,m,\theta_i} := e^{i(l-m)\theta_i}$ is invertible. Again, letting the array $\{(I_i, J_i)\}_{i=1}^M$ enumerate the index set $\{(I, J) : 1 \leq I \leq N, 1 \leq J \leq N\}$, i.e., $M = N^2$ complex (phased) measurements, we have

$$
\begin{aligned}
\tilde{L}_{lm} & \\
= & \frac{16R}{\pi} \sum_{J=1}^N \iota \left[\sum_{I=1}^N e^{2\pi i (l-m) I/N} \right] \frac{\cos \left(\left(m_0 + \frac{J-m}{2} \right) \pi \right) \cos \left(\left(m_0 + \frac{J-l}{2} \right) \pi \right)}{4m_0 + 2J + 1} + O(m_0^{-2}) \\
= & \frac{16RN}{\pi} \delta_{l,m} \begin{pmatrix} 1 & 0 \\ 0 & 1 \end{pmatrix} \sum_{J=1}^N \frac{\cos^2 \left(\frac{(J-m)\pi}{2} \right)}{4m_0 + 2J + 1} + O(m_0^{-2}).
\end{aligned}
$$

From here onward, the analysis is the same as in section 7.1.1 to get the same block matrix E such that for all $1 \leq l, m \leq N$,

$$\left(E^T \circ \tilde{L} \circ E \right)_{lm} = \frac{32RN}{\pi} \delta_{l,m} K_{\mathtt{mod}_2(m), m_0, [\frac{N-1}{2}]} \begin{pmatrix} 1 & 0 \\ 0 & 1 \end{pmatrix} + O(m_0^{-2}). \tag{7.22}$$

Now a similar argument as in section 7.1.1 applied to get an identical result for the phased reconstruction:

$$\kappa(\tilde{T}_{m_0}, \ker(C)) \leq \sqrt{\frac{m_0 + 2}{m_0 + 1}} + O(m_0^{-2}) \leq 1 + O(m_0^{-1}), \tag{7.23}$$

and by tracing all the constants, we can see the constants represented by big-O's is of the same magnitude as in the phaseless reconstruction. Therefore the ill-posedness in inverting T and $\tilde{T}$ are actually of the same order of magnitude using a same set of measurement angles, and the following result holds.

Theorem 7.3. *For a given target resolution N, the condition number $\kappa(\tilde{T}_{m_0}, ker(C))$ of the operator $\tilde{T}_{m_0}$ for $m_0 \in \mathbb{Z}$ can be controlled by*

$$\kappa(\tilde{T}_{m_0}, ker(C)) \leq 1 + O(m_0^{-1}) \tag{7.24}$$

if we make an N^2 complex (phased) measurement arrangement:

$$(\theta_i, \widetilde{\theta}_i, k_i) = \left(2\pi I_i/N, 2\pi I_i/N + \pi, \frac{4m_0 + 2J_i + 1}{8R} \right), \tag{7.25}$$

where $\{(I_i, J_i)\}_{i=1}^M$ enumerates through $\{(I, J) : 1 \leq I \leq N, 1 \leq J \leq N\}$.

Nonetheless, we notice a fundamental difference here between the phased and phaseless reconstructions. For the phased reconstruction, the matrix $\tilde{L}$ is invertible itself, therefore the constraint $Cx = 0$ is redundant. However, in the phaseless reconstruction, this set of constraints is necessary for us to get to a solution in the inversion process. Therefore, to fully exploit the constraints $Cx = 0$, it shall be possible to obtain the same stability estimate for $\hat{T}$ even if the number of equations represented by the matrix are cut off by half.

16

There are different ways to realize this, and we suggest one of them below. We shall not repeat all the details in the argument again but give only a sketch.

Suppose we choose the set of measurement points $(\theta_i, \widetilde{\theta}_i, k_i)$ as $\left(2\pi I_i/N, 2\pi I_i/N + \pi, \frac{4m_0 + 2J_i + 1}{8R}\right)$ where $\{(I_i, J_i)\}_{i=1}^M$ enumerate the index set $\{(I, J) : 1 \le I \le N/2, 1 \le J \le N\}$, but we only measure the real part of the far-field pattern $A_\infty^{\mathrm{meas}}(\theta_i, \widetilde{\theta}_i, k_i)$. Clearly, we have N^2 real (phased) measurements. From the fact that $P_R(\theta_i, \widetilde{\theta}_i, k_i)$ is real, we have

$$\mathrm{Re}\left(\tilde{T}\left[(\delta\,\mathfrak{F}[h])^{est}\right]\right) = \mathrm{Re}\left(G(A_\infty^{\mathrm{meas}}(\theta_i, \widetilde{\theta}_i, k_i))\right) = G\left(\mathrm{Re}(A_\infty^{\mathrm{meas}}(\theta_i, \widetilde{\theta}_i, k_i))\right). \tag{7.26}$$

Therefore, by taking only N^2 real (phased) measurements, we are actually dropping half of the equations representing measurements from the imaginary part. Now, in order to distinguish from the previous measurement setting, we denote the operator with these new measurement events as $\widetilde{\tilde{T}}_{m_0}$ for a given m_0.

With this very particular choice of real (phased) measurements, we know from (7.3) that the matrix $\widetilde{\tilde{T}}_{m_0}$ is coincidentally the same as T_{m_0}. Hence, if we write $\widetilde{\tilde{L}} := \widetilde{\tilde{T}}_{m_0}^T \widetilde{\tilde{T}}_{m_0}$, then $\widetilde{\tilde{L}} = L$. Therefore, with the same E as previously chosen, the same argument applies for us to get for all $1 \le l, m \le N$ that

$$\left(E^T \circ \widetilde{\tilde{L}} \circ E\right)_{lm} = \frac{64RN}{\pi}\delta_{l,m}K_{\mathtt{mod}_2(m),m_0,[\frac{N-1}{2}]} + O(m_0^{-2}). \tag{7.27}$$

This gives the following result.

Theorem 7.4. *An effective choice of only N^2 real phased measurement ensures the following bound for the condition number:*

$$\kappa(\widetilde{\tilde{T}}_{m_0}, ker(C)) \le 1 + O(m_0^{-1}). \tag{7.28}$$

Other ways to fully exploit the constraints $Cx = 0$ by dropping at most half of the equations represented by $\tilde{T}$, such as measuring the projection of complex number by another phase angle other than taking the real part, or taking only a special set of undersampling measurements, shall be possible, but for the sake of simplicity, we shall not proceed further.

From the above analysis, we can see that although the structures of T and $\tilde{T}$ are fundamentally different, they have similar behavior on their condition numbers. Yet the phaseless reconstruction is still much more ill-posed than the phased counterpart, owing to the following very simple yet important point. In the phaseless reconstruction, we shall also need to invert L by a regularized inversion process L_α^{-1}; however, in a phased reconstruction, such an inversion of L is unnecessary. Therefore, instability imposed by L exists only in the phaseless reconstruction. Considering this fact, the total regularized inversion of the phaseless reconstruction is still much more ill-posed than the phased counterpart, having its condition number being $1/\alpha$ times of the phased reconstruction.

8 Numerical experiments

In this section, we will first present numerical results illustrating some behaviors of the condition number $\kappa(T_{m_0}, \ker(C))$ using our measurement strategy described in the section 7.1, then focus on the inverse problem of shape reconstruction from the observed magnitude of far-field data.

8.1 Condition number of T subjected to $Cx = 0$

In what follows, we shall observe the behaviors of the condition number $\kappa(T_{m_0}, \ker(C))$ using our measurement strategy given in Theorem 7.3 and check the asymptotic estimate of $\kappa(T)$ in the theorem as m_0 grows. With a given m_0, we now fix the resolution $N = 51$ and choose the wave-numbers k such that $k = \frac{4m_0 + 2J + 1}{8R}$ with $R = 0.2$ and $J = 5, ..., 10$. The measurement points are the same as stated in Theorem 7.3. We compute the condition number of the operator T with $m_0 = 1, ..., 20$. The values of the corresponding condition numbers are plot in Figure 1.
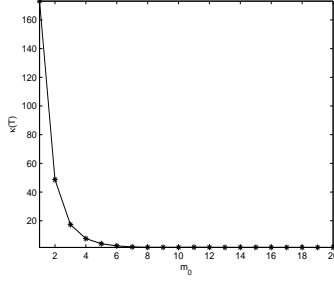
Figure 1: Decay of $\kappa(T, \ker(C))$ with respect to m_0.

We see clearly the drastic decay of the condition number as m_0 grows, showing the effectiveness of increasing stability by the increment of m_0. This agrees with the result we obtained in Theorem 7.3.

8.2 Phaseless reconstruction

We shall now proceed to present several numerical examples to show the performance of the newly proposed reconstruction algorithm, i.e., Algorithm 2 in Section 6.1, from phaseless far-field data. In order to attain robustness and stability of our algorithm, we approximate the inversion of L in Step 2 by L_α as in section 7.2 for some regularization α described below.

In the following 3 examples, we consider an infinite homogeneous background medium with its material coefficient being 1. In each example, an inhomogeneous inclusion $D = B^\delta$ is then introduced as a perturbation of a circular domain $B = B(0, R)$ for some $\delta > 0$ and its radius $R = 0.2$ sitting inside the homogeneous background medium, with its contrast always set to be $\varepsilon^* = 0.05$.

Given a domain B^δ, we first obtain the observed data of the forward problem, namely the magnitude of far-field data. In order to generate the far-field data for the forward problem and the observed scattering coefficients, we use the SIES-master package developed by H. Wang [54]. For a fixed wave-number k, we first solve for the solutions (ϕ_m, ψ_m) of (2.8) for $|m| \le 50$ using the rectangular quadrature rule with mesh-size $s/1024$ along the boundary of the target, where s denotes the length of the inclusion boundary. The scattering coefficients of B^δ of orders (n, m) for $|n|, |m| \le 50$ are then calculated, and the far-field data $A(\theta_d, \theta_x, k)$ is evaluated using (2.10) with $\theta_d, \theta_x \in (0, 2\pi]$ on a uniform mesh of size $N = 50$. Then the magnitude of the far-field pattern $|A(\theta_d, \theta_x, k)|$ is taken for our reconstruction process. In order to test the robustness of our reconstruction algorithm against the noise, we introduce some multiplicative random noise in the magnitude of far-field pattern $|A(\theta_d, \theta_x, k)|$ point-wisely in the form:

$$|A^{\mathrm{meas}}(\theta_d, \theta_x, k)|^\sigma = |A^{\mathrm{meas}}(\theta_d, \theta_x, k)|(1 + \sigma\,\xi) \tag{8.1}$$

where ξ is uniformly distributed between $[-1, 1]$ and σ refers to the relative noise level. In the following 4 examples, we always set the noise level to be $\sigma = 5\%$.

Then we apply our reconstruction algorithm for shape reconstruction with the noisy phaseless data as $T^{-1} \circ L_\alpha^{-1} \circ F$ following the notation introduced in section 7, where the regularization parameter is chosen as $\alpha = 10^{-3}$. In view of (7.18), we make the choice of measurements such that the measured wave-numbers k satisfy $k = \frac{4m_0 + 2J + 1}{8R}$ with $m_0 = 10$ in all the examples, and $J = 5, ..., 5 + \tilde{C}$ for some $\tilde{C}$ to be chosen in each of the example. The relative error of the reconstruction is defined by

$$\text{Relative Error} := \frac{\text{Area}\left((D^{\mathrm{approx}} \bigcup D) \backslash (D^{\mathrm{approx}} \bigcap D)\right)}{\text{Area}(D)}, \tag{8.2}$$

where D^{approx} is the reconstructed domain of the exact one D. To demonstrate the effectiveness of our algorithm and illustrates the necessity of a certain number of measurements angles in the phaseless reconstruction (i.e. to test its resolution limit), we shall try 3 different sets of measurements angles:

Set 1 Full measurement angles (over-abundant number of measurements):

$$((\theta_d)_i, (\theta_x)_i) = (2\pi I_i/N_0, 2\pi K_i/N_0)\,, \quad 1 \le I_i, K_i \le N_0\,, \tag{8.3}$$

when N_0 is always chosen as 50 in all the examples;

18

Set 2 Transmission measurement angles (critical number of measurements):

$$((\theta_d)_i, (\theta_x)_i) = (2\pi I_i/N, 2\pi I_i/N + \pi + U), \quad 1 \leq I_i \leq N, \tag{8.4}$$

where $N := \min\{N : [\mathfrak{F}(h)](k) = 0, \quad |k| > N\}$ and h is the perturbation in the corresponding example and $U = (-\frac{\pi}{5}, \frac{\pi}{5})$;

Set 3 Half of transmission measurement angles (insufficient number of measurements):

$$((\theta_d)_i, (\theta_x)_i) = (2\pi I_i/[[N/2]], 2\pi I_i/[[N/2]] + \pi + U), \quad 1 \leq I_i \leq [[N/2]], \tag{8.5}$$

which consists of $[[N/2]]$ measurement angles, where N is the same as previously mentioned and $[[\cdot]]$ is the ceiling function.

The purpose of introducing an interval U instead of one single point is to increase numerical stability in reconstruction. We emphasize that **Sets 2** and **3** are set up only to test the resolution limit of our phaseless reconstruction algorithm. We are not suggesting the necessity to determine $\min\{N : [\mathfrak{F}(h)](k) = 0, |k| > N\}$ from h before utilizing our algorithm. Such information is unnecessary and unavailable in a practical phaseless reconstruction.

In order to further increase numerical stability using a critical number of measurements (**Set 2**) and an insufficient number of measurement (**Set 3**), we further regularize our inversion process by a L^1 regularizer to enforce sparsity in the Fourier modes of our reconstructed perturbation, i.e., we solve

$$\min_{C\mathbf{X}=0} ||(L_\alpha \circ T)\mathbf{X} - F(|A_\infty^{\text{meas}}(\theta, \widetilde{\theta}, k)|)||_2^2 + \beta||\mathbf{X}||_1 \tag{8.6}$$

where β is a regularization parameter that is always chosen as $\beta = 0.05$. We perform the L^1 minimization by a standard Bregman iteration [20].

Example 1. In this example, we consider an inhomogeneous domain of a flori-form shape $D = B^\delta$ described by the following parametric form (with $\delta = 0.1$ and $n = 3$):

$$r = 0.2(1 + \delta \cos(n\theta)), \quad \theta \in (0, 2\pi], \tag{8.7}$$

which is a perturbation of the domain $B = B(0, 0.2)$; see Figure 2 (left) and (right) respectively for the shape of the domain and the contrast of the inhomogeneous medium.
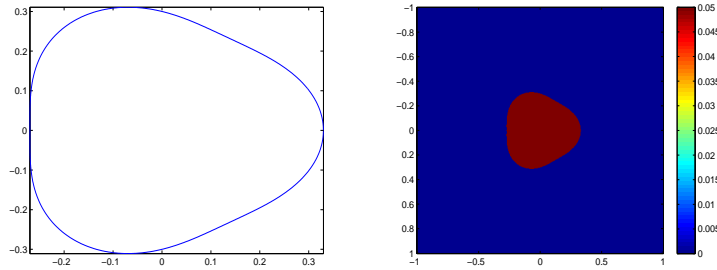

Figure 2: Exact inhomogeneous domain (left) and the contrast of the inclusion (right) in Example 1.

The magnitude of the far-field pattern for 6 wave-numbers are used for shape reconstruction, i.e. $\tilde{C} = 5$, and the Fourier coefficients of the reconstructed perturbations using the respective measurement sets are shown in Figure 3.
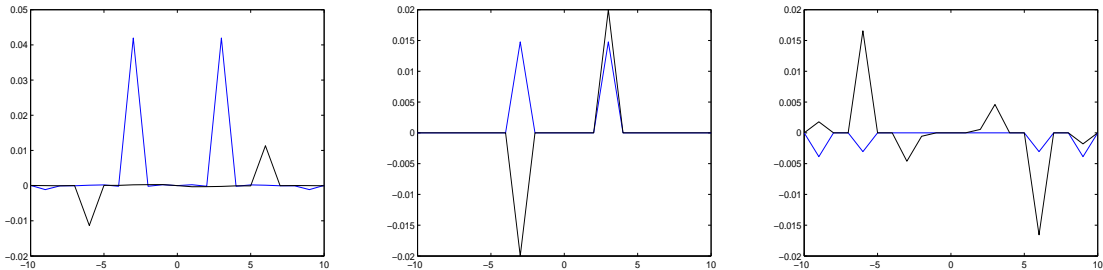
Figure 3: Fourier coefficients of reconstructed perturbations in Example 1; **Set 1** to **Set 3** from left to right; blue: real part; black: imaginary part.

Although there are some deficiencies in the reconstruction of Fourier modes, we can see from these figures the Fourier coefficients reconstructed from **Set 1** is largest at $|n| = 3$ with its magnitude almost between 0.04 and 0.05, which clearly indicates a strong dominance of $\delta \cos(3\theta)$ with magnitude δ between 0.08 and 0.1 and corresponds to the signal from the exact inclusion. The reconstruction from **Set 2** has more deficiency, that the Fourier mode is somehow shifted to $\delta(\cos(3\theta) + \sin(3\theta))$ with magnitude δ between 0.02 and 0.025. However, the location of the peak Fourier mode is still correct. Nonetheless, the reconstruction from **Set 3** deviates totally from the exact solution, indicating its insufficiency in number of measurements to reconstruct the perturbation. This goes with the theoretical analysis in section 7.1.1.

Now we show in Figure 4 (top) the shapes of reconstructed domains, Figure 4 (middle) the contrast of the reconstructed media and Figure 4 (right) a comparison between the reconstructed domains D^{approx} and exact domain D using the values of a sum of characteristic functions $\chi_D + \chi_{D^{\mathrm{approx}}}$. The relative L^2 errors of the reconstructions for **Set 1** to **Set 3** are respectively 3.29%, 6.34% and 11.72%. In view of the severe ill-posedness of the phaseless reconstruction problem and 5% percent of measurement noise, the reconstructions from **Set 1** and **Set 2** measurements are quite reasonable
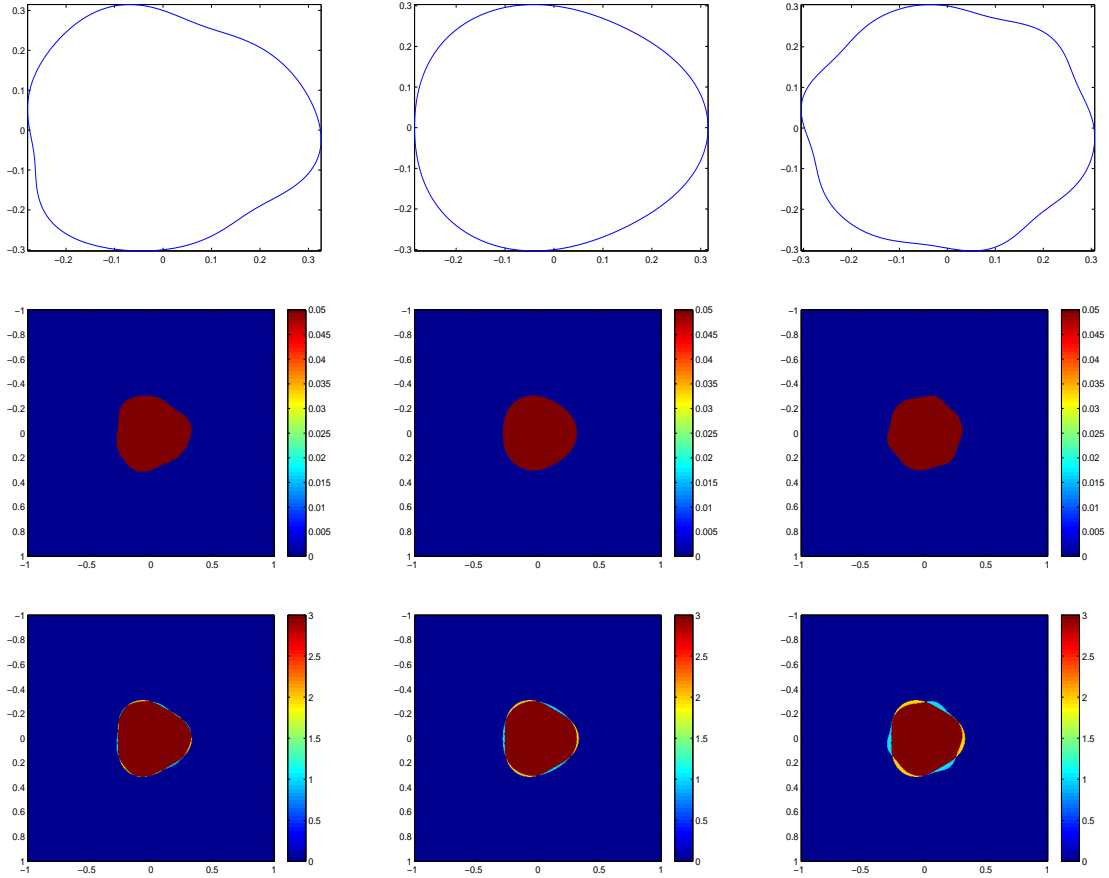

Figure 4: Reconstructed domain and medium in Example 1 and comparison between the exact and reconstructed domains; **Set 1** to **Set 3** from left to right; from top to bottom: reconstructed shape, reconstructed inclusion, and comparison between reconstructed and exact domains.

Example 2. We test another domain of the flori-form shape described by (8.7) with $\delta = 0.1$ and $n = 5$. Figure 5 (left) and (right) show the shape of the domain and the contrast of the inhomogeneous medium respectively.
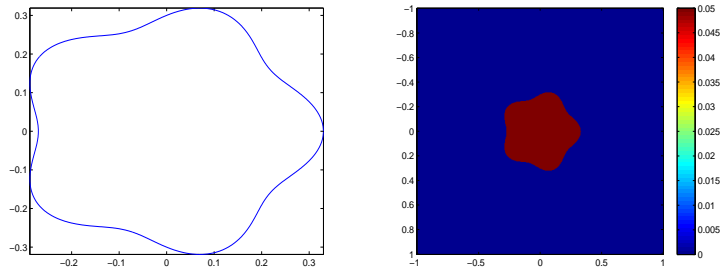
Figure 5: Exact inhomogeneous domain (left) and the contrast of the inclusion in Example 2.

In this example, the magnitude of the far-field pattern for 16 wave-numbers are used for shape reconstruction, i.e. $\tilde{C} = 15$. The Fourier coefficients of the reconstructed perturbations using the respective measurement sets are shown in Figure 6.
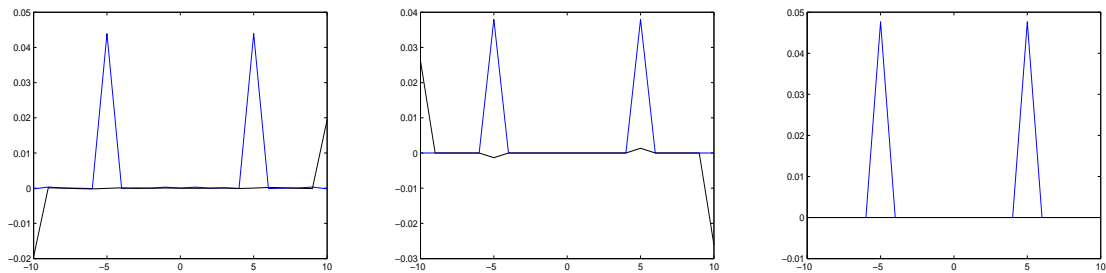

Figure 6: Fourier coefficients of reconstructed perturbations in Example 2; **Set 1** to **Set 3** from left to right; blue: real part; black: imaginary part.

We can now see that both the reconstructions from **Set 1** and **Set 2** are reasonable and indicate the correct peak Fourier modes and its magnitude. It is no surprise to see the reconstruction for **Set 2** is worse than that for **Set 1**. However we can see that in this particular case, the reconstruction for **Set 3** coincidentally collides with the exact solution after regularization.

In Figure 7 (top), (middle) and (right), the shapes of reconstructed domains, the contrast of the reconstructed media and the comparison between the reconstructed domains D^{approx} and exact domain D (by showing a sum of characteristic functions $\chi_D + \chi_{D^{\mathrm{approx}}}$) are presented respectively. The relative L^2 errors of the reconstructions for **Set 1** to **Set 3** are respectively 4.91%, 6.94% and 0.57%. As we mentioned above, quite surprisingly, the L^1 regularizer coincidentally provides a very good estimate for **Set 3**.
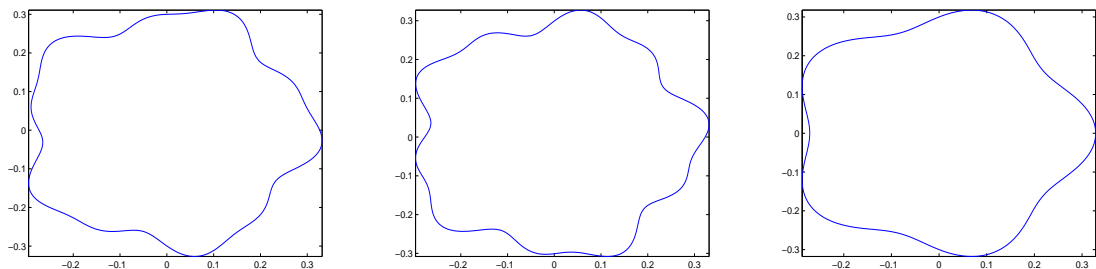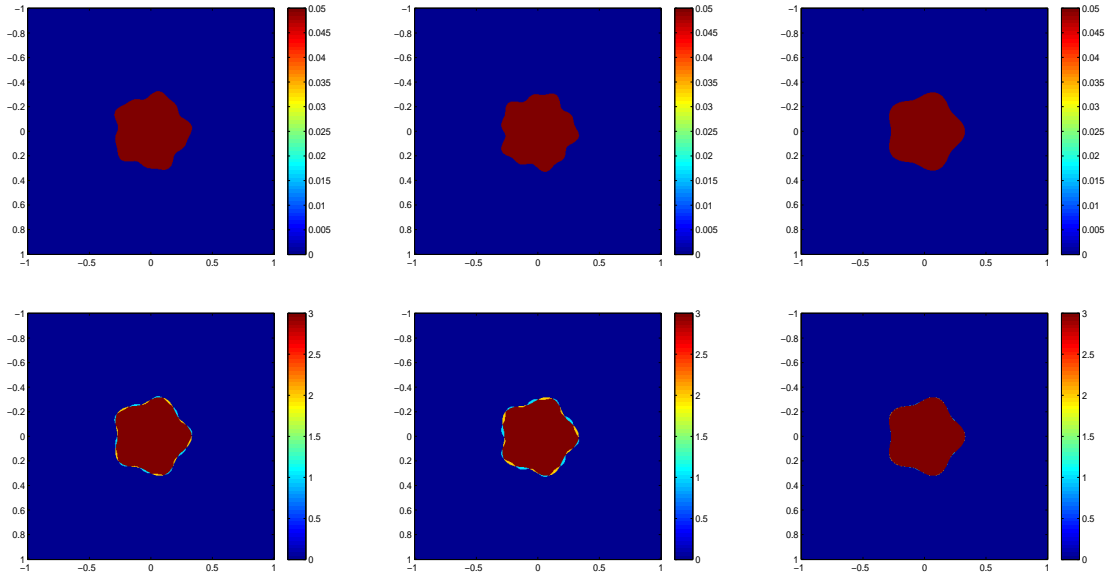
Figure 7: Reconstructed domain and medium in Example 2 and comparison between the exact and reconstructed domains. **Set 1** to **Set 3** from left to right; reconstructed shape, reconstructed inclusion and comparison between reconstructed and exact domains from top to bottom.

Example 3. In this last example, we test a domain of more complicated flori-form shape $D = B^\delta$ described by the following parametric form (with $\delta = 0.1$ and $n = 3$):

$$r = 0.2(1 + \delta \cos(n\theta) + 2\delta \cos(2n\theta)), \quad \theta \in (0, 2\pi], \tag{8.8}$$

The shape of the domain is given in Figure 8 (left) and the contrast of the inhomogeneous medium in Figure 8 (right).
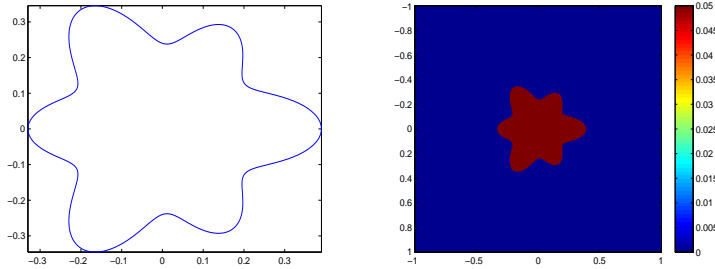

Figure 8: Exact inhomogeneous domain (left) and contrast of the inclusion (right) in Example 3.

The magnitude of far-field pattern for 6 wave-numbers are used for shape reconstruction, i.e. $\tilde{C} = 5$, and the Fourier coefficients of the reconstructed perturbations using the respective measurement sets are shown in Figure 9.
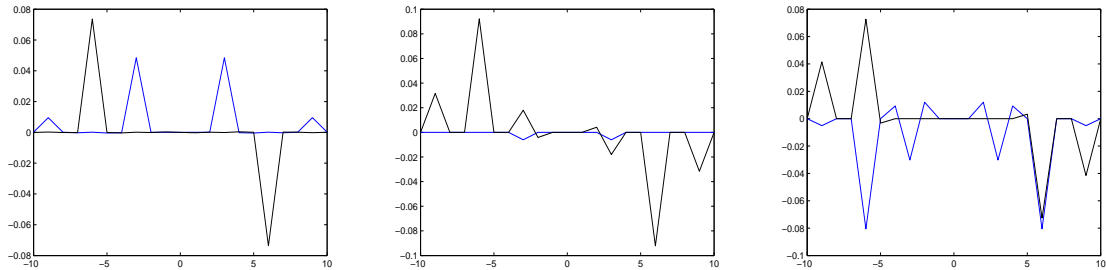
Figure 9: Fourier coefficients of reconstructed perturbations in Example 3; **Set 1** to **Set 3** from left to right; blue: real part; black: imaginary part.

In this example, as we can see, the reconstructions from **Set 1** is the best, with both the peak Fourier modes and their magnitudes quite close to the exact one, although with some phase shifts. Reconstruction from **Set 2** is still reasonable. The magnitude of the 6-th Fourier modes is closer to the exact one, however that of the 3-th mode deviates further from the exact one, and they have more phase shifts. Reconstruction from **Set 3** is the worst, with great deficiency from the exact perturbation, considering the fact this reconstruction gives us many modes that do not exist in the exact perturbation.

In Figure 10 (top), (middle) and (right), the shapes of reconstructed domains, the contrast of the reconstructed media and a comparison between the reconstructed domains D^{approx} and exact domain D are presented respectively The relative L^2 errors of the reconstructions for **Set 1** to **Set 3** are respectively 11.61%, 13.48% and 14.84%. This indicates that the reconstruction for **Set 1** is the best, that for **Set 2** is still good, and that for **Set 3** is the worst. This goes with the theory we discussed in section 7.1.1.
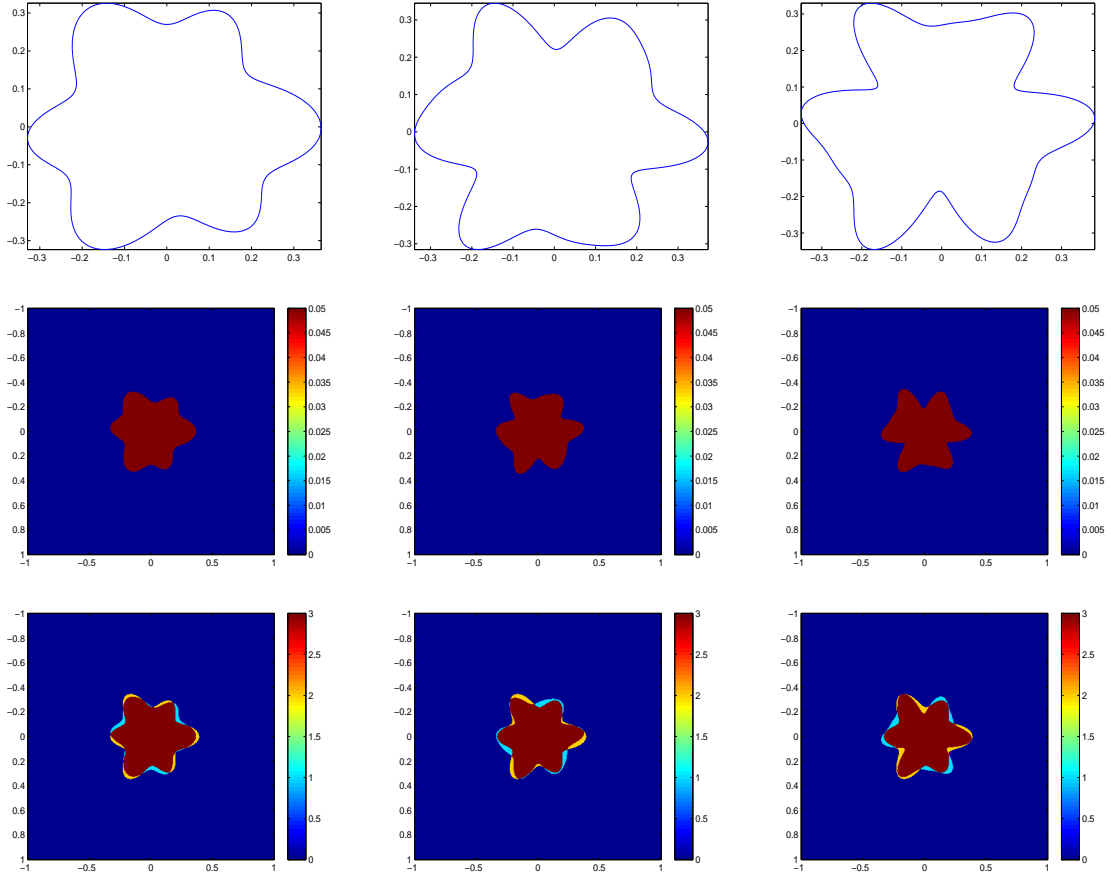

Figure 10: Reconstructed domain and medium in Example 3 and comparison between the exact and reconstructed domains; **Set 1** to **Set 3** from left to right; reconstructed shape, reconstructed inclusion and comparison between reconstructed and exact domains from top to bottom.

The reconstructions for **Set 1** (over-abundant number of measurements) and **Set 2** (critical number of measurements) are quite reasonable, considering the severe ill-posedness of the phaseless reconstruction problem and a 5% percent measurement noise.

References

[1] M. Abramowitz and I.A. Stegun, Handbook of Mathematical Functions, Dover Publications, 1970, 365-366.

[2] A. Abubakar and P. M. van den Berg, *The contrast source inversion method for location and shape reconstructions*, Inv. Prob. 18 (2002), 495-510.

[3] A. Abubakar, P. M. van den Berg, and J.J. Mallorqui, *Imaging of biomedical data using a multiplicative regularized contrast source inversion method*, IEEE Trans. Microw. Theory Tech. 50 (2002), 1761-1771.

[4] A. Abubakar, P. M. van den Berg, and J.T. Fokkema, *Time-lapse TM-polarization electromagnetic imaging*, Int. J. Subsurface Sens. Tech. Appl. 4 (2003), 117-135.

[5] H. Ammari, Y.T. Chow and J. Zou, *Super-resolution in imaging high contrast targets from the perspective of scattering coefficients*, Preprint 2015.

[6] H. Ammari, Y.T. Chow and J. Zou, *The concept of heterogeneous scattering coefficients and its application in inverse medium scattering*, SIAM J. Math. Anal. 46 (2014), 2905-2935.

[7] H. Ammari, J. Garnier, H. Kang, M. Lin, S. Yu, *Generalized polarization tensors for shape description*, Numer. Math. 126 (2014), 119-224.

[8] H. Ammari, H. Kang, H. Lee, and M. Lim, *Enhancement of near-cloaking. Part II: the Helmholtz equation*, Comm. Math. Phys. 317 (2013), 485-502.

[9] H. Ammari, M.P. Tran, and H. Wang, *Shape identification and classification in echolocation*, SIAM J. Imag. Sci. 7 (2015), 1883–1905.

[10] G. Bao and P. Li, *Inverse medium scattering for the Helmholtz equation at fixed frequency*, Inv. Prob. 21 (2005), 1621-1641.

[11] K. Belkebir and M. Saillard, *Special section: Testing inversion algorithms against experimental data* Inv. Prob. 17 (2001), 1565-1571.

[12] E.J. Candes, X.Li, M. Soltanolkotabi, *Phase Restrieval from coded diffraction patterns*, Appl. Comp. Harmonic Anal., 2014, in Press.

[13] E. J. Candes, T. Strohmer, V. Voroninski, *PhaseLift: Exact and Stable Signal Recovery from Magnitude Measurements via Convex Programming*, Commun. Pure Appl. Math. 66 (2013), 1241-1274.

[14] S. Caorsi, A. Massa, M. Pastorino and A. Randazzo, *Electromagnetic detection of dielectric scatterers using phaseless synthetic and real data and the memetic algorithm*, IEEE Trans. Geosci. Remote Sens. 41 (2003), 2745-2753.

[15] X. Chen, *Application of signal-subspace and optimization methods in reconstructing extended scatterers*, J. Opt. Soc. Amer. A 26 (2009), 1022-1026.

[16] X. Chen, *Subspace-based optimization method for solving inverse-scattering problems*, IEEE Trans. Geosci. Remote Sensing 48 (2010), 42-49.

[17] D. Colton and R. Kress, Inverse Acoustic and Electromagnetic Scattering ed., Springer Verlag, Berlin, 1998.

[18] . L. Crocco, M. D'Urso, and T. Isernia, *Faithful non-linear imaging from only-amplitude measurements of incident and total fields*, Optics Express 15 (2007), 3804-3815.

[19] T.J. Cui, Y. Qin, G.L. Wang and W.C. Chew, *Low-frequency detection of two-dimensional buried objects using high-order extended Born approximations*, Inv. Prob. 20 (2004), S41-62.

[20] J. Darbon, D. Goldfarb, S. Osher, W. Yin, Bregman iterative algorithms for l_1-minimization with applications to compressed sensing, SIAM J. Imag. Sci. 1 (2008), 143-168.

[21] L. Demanet, P. Hand, *Stable optimizationless recovery from phaseless linear measurements*, J. Fourier Anal. Appl. 20 (2014), 199-221.

[22] M. D'Urso, K. Belkebir, L. Crocco, T. Isernia, and A. Litman, *Phaseless imaging with experimental data: Facts and challenges*, J. Opt. Soc. Am. A . 25 (2008), 271-281.

[23] K. Ito, B. Jin and J. Zou, *A direct sampling method to an inverse medium scattering problem*, Inv. Prob. 28 (2012), 025003.

[24] O. Ivanyshyn and R. Kress, *Identification of sound-soft 3D Obstacles from phaseless data*, Inv. Prob. and Imag. 4 (2010), 131-149.

[25] A. Kirsch, *The MUSIC-algorithm and the factorization method in inverse scattering theory for inhomogeneous media*, Inv. Prob. 18 (2002), 1025-1040.

[26] M. V. Klibanov, *On the first solution of a long standing problem: uniqueness of the phaseless quantum inverse scattering problem in 3-d*, Appl. Math. Letters 37 (2014), 82-85.

[27] M. V. Klibanov, *Phaseless inverse scattering problems in three dimensions*, SIAM J. Appl. Math. 74 (2014), 392-410.

[28] M. V. Klibanov, L. H. Nguyen, K. Pan, *Nanostructures imaging via numerical solution of a 3-d inverse scattering problem without the phase information*, Preprint, arXiv:1404.1183.

[29] M. V. Klibanov and V. G. Romanov, *Explicit formula for the solution of the phaseless inverse scattering problem of imaging of nano structures*, J. Inv. Ill-Posed Prob., 2015, doi. 10.1515

[30] R. Kress and W. Rundell, *Inverse obstacle scattering with modulus of the far field pattern as data*, Inverse problems in medical imaging and nondestructive testing, Oberwolfach, 1996, 75-92.

[31] J. Li, H. Liu and J. Zou, *Multilevel linear sampling method for inverse scattering problems*, SIAM J. Sci. Comp. 30 (2008), 1228-1250.

[32] J. Li, H. Liu and J. Zou, *Strengthened linear sampling method with a reference ball*, SIAM J. Sci. Comp. 31 (2009), 4013-4040.

[33] L.L. Li, H. Zheng, and F. Li, *Two-dimensional contrast source inversion method with phaseless data: TM case*, IEEE Trans. Geosci. Remote Sens. 47 (2009), 1719-1736.

[34] C.W. Liao, M.A. Fiddy and C.L. Byrne, *Imaging from the zero locations of far-field-intensity data*, J. Opt. Soc. Am. A 14 (1997), 3155-3161.

[35] A. Litman and K. Belkebir, *Two-dimensional inverse profiling problem using phaseless data*, J. Opt. Soc. Am. A 23 (2006), 2737-2746.

[36] K. Liu, Y. Xu and J. Zou, *A parallel radial bisection algorithm for in verse scattering problems*, Inv. Prob. Sci. Eng. 21 (2013), 197-209.

[37] K. Liu, J. Zou, *A multilevel sampling algorithm for locating inhomogeneous media*, Inv. Prob. 29 (2013), 095003.

[38] S. Mallat, I. Waldspurger, *Phase retrieval for the Cauchy wavelet transform*, preprint, arXiv:1404.1183.

[39] E. A. Marengo, F. K. Gruber and F. Simonetti, *Time-reversal MUSIC imaging of extended targets*, IEEE Trans. Image Proc. 16 (2007), 1967-1984.

[40] R. Potthast, *A survey on sampling and probe methods for inverse problems*, Inv. Prob. 22 (2006), R1-R47.

[41] T. Takenaka, D. Wall, H. Harada and M. Tanaka, *Reconstruction algorithm of the refractive index of a cylindrical object from the intensity measurements of the total field*, Microw. Opt. Technol. Lett. 14 (1997), 182-188.

[42] C. Torresverdin and T.M. Habashy, *Rapid 2.5-dimensional forward modeling and inversion via a new nonlinear scattering approximation*, Radio Sci. 29 (1994), 1051-1079.

[43] R. Vershynin, *Introduction to the non-asymptotic analysis of random matrices*, Compr. Sensing, 2012, 210-268.

[44] P.M. van den Berg and A. Abubakar, *Contrast source inversion method: state of art*, Prog. Electromagn. Res. PIER 34 (2001), 189-218.

[45] P.M. van den Berg, A. Abubakar and J.T. Fokkema, *Multiplicative regularization for contrast profile inversion*, Radio Sci. 38 (2003), 23-1 - 23-10.

[46] P.M. van den Berg and R. E. Kleinman, *A contrast source inversion method*, Inv. Prob. 13 (1997), 1607-1620.

[47] P.M. van den Berg, A. L. van Broekhoven and A. Abubakar, *Extended contrast source inversion*, Inv. Prob. 15 (1999), 1325-1344.

[48] G. N. Watson, A treatise on the theory of Bessel functions (2nd.ed.), Cambridge University Press (1966).

[49] G. N. Watson, Theory of Bessel Functions, 2nd edition, Cambridge University Press (1944).

[50] M.S. Zhdanov and S. Fang, *Three-dimensional quasi-linear electromagnetic inversion*, Radio Sci. 31 (1996), 741-754.

[51] M.S. Zhdanov and G. Hursan, *3D electromagnetic inversion based on quasi-analytical approximation*, Inv. Prob. 16, (2000), 1297-1322.

[52] H. Zheng, L. Li, and F. Li, *A multi-frequency MRCSI algorithm with phaseless data*, Inv. Prob. 25 (2009),1-13.

[53] H. Zheng, M.-Z. Wang, Z. Zhao, and L. Li, *A novel linear EM reconstruciton algorithm with phaseless data*, Progress In Electromagnetics Research Letters 14 (2010), 133-146.

[54] http://www.math.ens.fr/~hanwang/software/examples/Helmholtz_R2/demo.html

Recent Research Reports

Nr.	Authors/Title

2015-26   C. Hafner and R. Hiptmair and P. Souzangar
Data Sparse Numerical Models for SNOM Tips

2015-27   F. Leonardi and S. Mishra and Ch. Schwab
Numerical approximation of statistical solutions of incompressible flow

2015-28   P. Chen and Ch. Schwab
Model Order Reduction Methods in Computational Uncertainty Quantification

2015-29   G. S. Alberti and S. Dahlke and F. De Mari and E. De Vito and S. Vigogna
Continuous and discrete frames generated by the evolution flow of the Schrödinger
equation

2015-30   P. Grohs and G. Kutyniok and J. Ma and P. Petersen
Anisotropic Multiscale Systems on Bounded Domains

2015-31   R. Hiptmair and L. Scarabosio and C. Schillings and Ch. Schwab
Large deformation shape uncertainty quantification in acoustic scattering

2015-32   H. Ammari and P. Millien and M. Ruiz and H. Zhang
Mathematical analysis of plasmonic nanoparticles: the scalar

case

2015-33   H. Ammari and J. Garnier and L. Giovangigli and W. Jing and J.K. Seo
Spectroscopic imaging of a dilute cell suspension

2015-34   H. Ammari and M. Ruiz and S. Yu and H. Zhang
Mathematical analysis of plasmonic resonances for nanoparticles: the full Maxwell
equations